Elisabeth Rogl, BSc

Spatial Rocking in a photorefractive cavity

MASTER THESIS

For obtaining the academic degree
Diplom-Ingenieurin

Master Programme of
Technical Physics

Graz University of Technology

Supervisor:

Ao. Univ.-Prof. Dipl.-Ing. Dr.techn. Laurentius Windholz

Institute of Experimental Physics

in cooperation with the University of Valencia

Graz, March 2014

Contents

This Master´s Thesis has been realized in collaboration with the Optical Department of the University of Valencia under the supervision of Fernando Silva Vázquez.
The aim of the thesis was the experimental realization of a technique called Spatial Rocking. The theory of the Spatial Rocking was published in [1]. The equations predict phase bistability in spatially extended self-oscillatory systems and the dissipative structures associated with it.

The optical system employed to study the Spatial Rocking was a photorefractive cavity in linear configuration with large Fresnel number.
This kind of optical cavity shows certain advantages from the experimental point of view as it is a comparably simple system concerning the experimental setup and doesn´t require expensive equipment for signal analysis and processing.

Because of serious technical problems the planned experiment couldn´t be carried out. Thus this thesis contains the theoretical description of the planned experiment and a description of the experimental setup.

CHAPTER 1

Introduction

The spatial Rocking is a modification of the originally developed temporal Rocking.
For both types one can say that Rocking is an alternative forcing technique to introduce phase bistability in spatially extended self-oscillatory systems that are insensitive to conventional methods of bistable phase locking.
The name Rocking comes from a qualitative discussion of a very simple case to illustrate how the mechanism alter a system´s potential. In this pictorial picture the potential gets rocked along an axis in phase space which leads to the observed bistability of the systems state.

The patterns associated with this phase bistability are optical dissipative structures and are the nonlinear dynamic response of the system to the forcing. Under certain circumstances those structures become stable and stationary.
Such nonlinear structures are more complex and thus more interesting than structures due to linear processes. Especially bistable systems exhibit structureful patterns.

Nonlinear optical cavities (e.g. laser cavities) provide a good possibility to study spontaneous pattern formation.
Investigation in this sector is of high interest from the fundamental point of few but is also of high technological interest.
The application of the Rocking technique in a nonlinear optical cavity introduces optical phase bistability which leads to the possible formation of stable optical phase patterns in the transversal plane of the laser light including cavity solitons.
In this sense the Rocking is a versatile instrument to produce transportable information that doesn´t get changed on its way to the receiver for the signals formed by that way constitute a stable structure.

The two types of Rocking, temporal and spatial, refer to the kind of modulation (temporal, spatial) of the amplitude of the as Rocking beam into the optical cavity injected force. This will be explained in more detail in the concerning section. But here the importance of the new technique of the spatial Rocking should become clear.

The temporal rocking uses an injection with amplitude modulated in time. This modulation frequency of the Rocking beam can be too close to eventual relaxation oscillations in certain optical cavities (class B lasers). Resonance phenomena can affect the mechanism of bi-stabilization of the system. This gives motivation for the spatial rocking, where the Rocking beam is spatially modulated and thus resonance phenomena can be avoided.

This Master´s thesis is divided into the following parts :

The first section is an introduction to pattern formation and focuses on dissipative structures. Dissipative structures are the kind of structures we were dealing with. The characteristics and conditions of formation are discussed in sections 1.2.1 and 1.2.2, followed by some examples in nature (section 1.3) and a short review of how scientific interest in optical patterns arose (section 1.4). An introduction to the mathematical description of dissipative systems is given in section 1.5 and section 1.6 presents particular solutions, namely localized structures.
Optical vortices and cavity solitons are localized structures in optical systems and are described in section 1.6.1.

A more detailed mathematical description of phase invariant and phase locked systems which show these types of structures can be found in sections 1.7 and 1.8, respectively.

The conversion of a phase invariant into a phase locked system is discussed in section 1.9. Rocking (temporal and spatial) as alternative method to the parametric forcing is presented in sections 1.9.2 and 1.9.3.

The chapter about Nonlinear optical cavities (NLOCs), chapter 2, presents the experimental realization of the theory in optical systems. After a general description of NLOCs a particular type of resonator which represents well the theory is discussed in more detail (section 2.2).

There is a large sections dedicated to photorefractive nonlinear optics (section 2.3) as a $BaTiO_3$ crystal was used as active medium in our setup.

Finally the experiment which was supposed to be realized within this Master´s thesis will be described in chapter 2.5.

1.1 Patterns

Pattern formation is a dynamical process that happens in spatially extended nonlinear systems after a phase transition has taken place due to changes of external parameters.
The stationary spatially homogenous initial state becomes instable and can recover stability by the formation temporal, spatial or spatiotemporal oscillating state.
In mathematics this is described by the rupture of the translation symmetry by a bifurcation and a structure of specific length and time scale is formed [20].

The character of the patterns depends on many factors.
Nontrivial spatio-temporal structures are found in nonlinear dissipative systems, where they are formed spontaneously and constitute a stable dynamic state of the system.
Dissipative systems show a greater variety of structures than conservative systems. And within the dissipative systems the ones with broken phase symmetry show the more interesting patterns.

Nature is a dissipative system and there are lots of examples of natural patterns.
In science there´s also systems found that exhibit ordered structures of high complexity.
In laser physics appropriate conditions for spontaneous pattern formation are given in nonlinear optical cavities and even in society one can talk of dissipative structures.

For technological applications but also from fundamental point of view, dissipative structures in optics are of high interest.

Figures 1.1 and 1.3 show examples of structures in conservative and dissipative systems in nature and optics.

Figure 1.1: Examples of dissipative (left) and conservative (right) structures in nature.
left column: ice crystals, [24], right column: soliton in a water canal, [2]

Figure 1.2: A soliton wave in water [27].

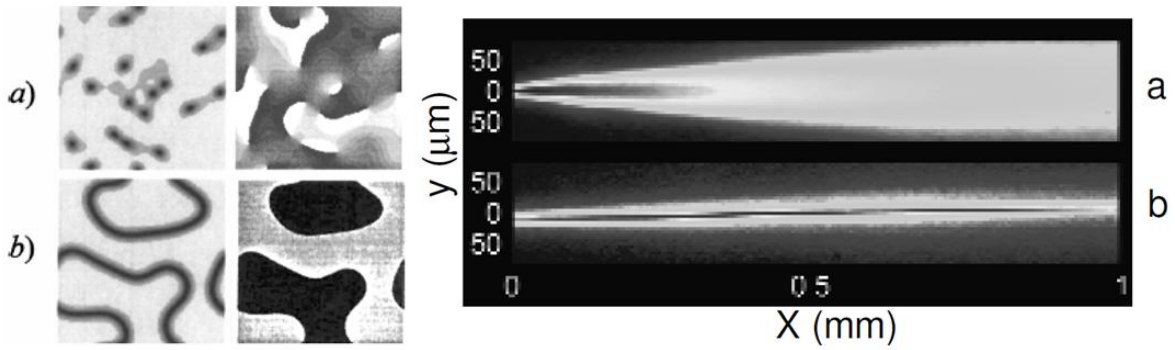

Figure 1.3: Examples of dissipative (left) and conservative (right) structures in optics.
left column: dissipative structures in the transverse plane of the light in a nonlinear optical cavity:(a) vortices in a phase invariant systems, (b) solitons in a phase bistable system, right column: an optical soliton (b) constitutes a stable structure as the beam of light does not suffer dispersion like in (a). Images taken from [2].

1.2 Dissipative Structures

1.2.1 What is a dissipative structure and where can it appear?

Dissipative structures are ordered structures that under certain circumstances can appear spontaneously in thermodynamically open non equilibrium systems. Such dissipative systems exchange energy and/or matter with the environment and work - often far - out of the thermodynamic equilibrium.

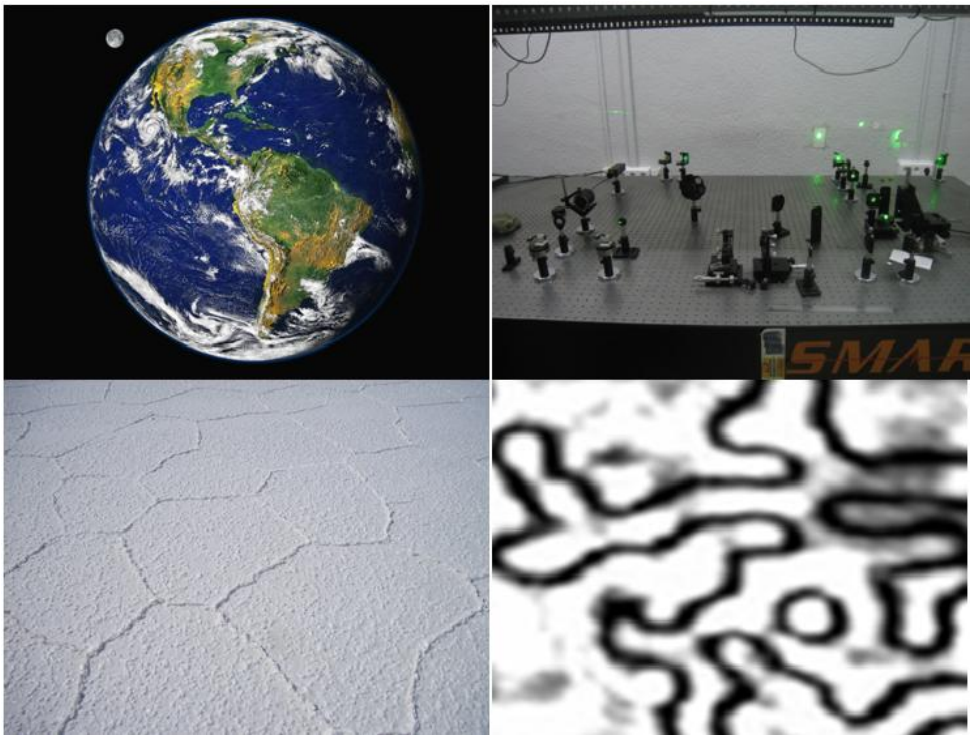

Figure 1.4: Examples for dissipative Systems and patterns.
Left column: The earth and its atmosphere and the structured surface of a salt lake.
Right column: A photorefractive oscillator and domain walls in the transverse plane of the light inside the resonator. Images taken from [26]

The dissipative structures are a phenomenon of spontaneous self organization within thermodynamically open non equilibrium systems, showing ordered dynamic behaviour that is in some sense a reproducible steady state.

In 1967 Prigogine suggested to call the stable spatial, temporal or spatiotemporal structures, that appear at far non-equilibrium above critical values of certain parameters of a thermodynamical open system in the nonlinear regime of the system´s response, dissipative structures.
They are characterized by relatively high stability against small perturbances and the hypercritical distance from equilibrium. The stability of the dissipative structures is due to a balance of nonlinearity and energy dissipation [20].

Patterns appear whenever the system is in an originally stable state and gets disturbed. To recover stability it reorganizes itself [11]. The concerning field of investigation is called *pattern*

formation.

There´s several pattern forming systems in nature (see section 1.3) and physics. Dissipative Structures can appear in chemical, biological and physical systems as long as certain prequesites are provided by the system (see section 1.2.2). Also optical systems display dissipative structures (see chapter 1.4).

1.2.2 Conditions for the formation of dissipative structures

Now one can ask himself: Which of the properties of all systems (biological, chemcial, physical) that show spontaneous pattern formation are specific for the system and wich are of general character?

All those systems have the following porperties in common:

- they are extended systems, where the scale of the structure is much smaller than the system in at least one dimension
- they are open, so that they can exchange energy with their environment (dissipative systems)
- there is an external force that pushes the system far out of equilibrium
- they respond in a nonlinear way to the external force with a spontanous break of symmetry of their inicial equilibrium state to recover stability

In thermodynamic systems pattern formation can be described by entropy considerations:

Thermodynamic equilibrium is defined for thermodynamically closed systems and characterized by maximum entropy, that´s maximum disorder. Any kind of structure implies non maximum entropy.
Following the second law of thermodynamicy an ordered state isn´t stable in a closed system. Thus stable structures are only possible in thermodynamically open systems.

A thermodynamically open system can show order due to the possibility to export entropy. The entropy can locally reduce due to pattern formation. Since the total entropy doesn´t reduce the process doesn´t contradict the second law of thermodynamics. If the system is dissipative it can go into a state with zero total entropy production $dS_{tot} = dS_i + dS_{ext}$, when the entropy produced within the system is given to the environment $dS_{ext} = -dS_i$. This constitutes a stationary nonequilibrium state.

The charactersitics of pattern forming systems in nature listed above can be found in optics as well. In specific in nonlinear optical cavities. Furthermore there is several analogies found between thermodynamics and optics (see section 1.4 and chapter 2).
Thus one can talk of dissipative strucutures in optics, which provides the possibility of scientific investigation of dissipative structures apart from technological applications. The information for this section is taken from [9], [23] and [20].

1.3 Patterns in Nature

The formation of dissipative structures is of fundamental importance for the formation of structures in nature and therefore for the possibility of evolution.
The earth and it´s atmosphere provide the prerequesites (1.2.2) to show dissipative structures. It is an open dissipative system as it converts solar radiation energy into heat and the processes are highly nonlinear.
Natural dissipative structures can easily be observed. Examples are clouds, rivers, hurricanes, dunes or the hexagonal structure formed on a salt lake (see figures 1.6 and 1.1).
Also creatures are considered dissipative structures. Celular structures, finger prints, the patterns on animal´s fur like the stripes of a cebra or the sprinkled leopard´s fur are only a few examples (see figure 1.5).
But also in natural systems not so obvious to be recognized by human beings ordered structures can appear. This is for example the alveolar structure formed in a bottom heated fluid (Bénard-Effect) or biochemical dynamic equilibrium.

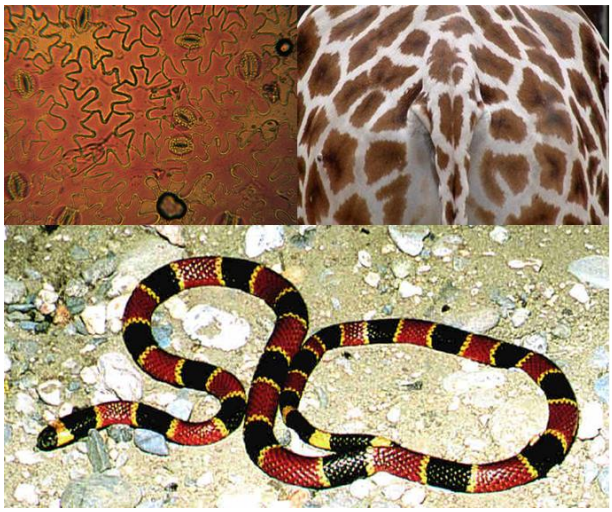

Figure 1.5: Examples of dissipative structures in flora and fauna. Above left: Cells of a Cyclamen flower . Above right: fur of a Giraffe. Below: A coral snake. Images taken from [25].

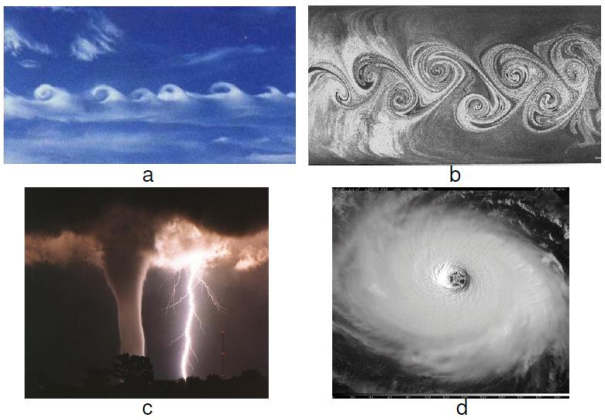

Figure 1.6: Examples of dissipative structures in the atmosphere. Clouds forming natural vortices under the action of wind. Images taken from [2].

1.4 Patterns in Optics

The interest in optical patterns arrose with the possibility of investigation when the first laser was developed. The studies of pattern formation in nonlinear optical cavities were influenced by the general ideas developed by Prigogine.

The properties of pattern forming systems mentioned in section 1.2.2 can be found in nonlinear optical cavities, that are excited out of resonance.

1.4.1 Historical review of patterns in optics

1960: With the developement of the first laser the studies of the formation of structures in the transversal plane of propagation of the laser light began. At that time the structures where considered disturbing and were suppressed by putting adequate diaphragms into the laser cavity to achieve most clean beams.

1970: Studies in broad-aperture lasers and first conections of laser physics with fluid and superfluid dynamics [12]. Later many more analogies between optics and hydrodynamics were found.

1980: At the beginning of the 80´s the interest into the studies realized in the 70´s grew and at the and of the 80´s investiagtions of optical patterns started.
There were theoretical studies made to obtain order parameter equations for the case of positive detuned lasers.
Those studies didn´t indicate the formation of extented patterns because extended patterns only appear in the case of negative detuning.

First experimental studies were realized in laser cavities of low Fresnel number. This was because high Fresnel numbers were difficult to realize. Thus the interesting essentially nonlinear patterns couldn´t be observed.

1990: Several important works on the issue were publicated.
Some of the most relevant pioneer works are:

- the study of the formation of brilliant solitons in free propagation [13]
- the prediction of patterns in lasers as nontrivial stationary solutions [14], [15]
- the appearance of vortices in the Maxwell-Bloch equations [16]

Well studied optical systems are the Kerr-cavity and the optical parametric oscillators (OPOs), but one of the most studied optic systems is the fotorefractive oscillator and its diverse variations. In those systems high Fresnel numbers were realized for the first time using self-imaging configurations, which permitted the study of spatio-temporal dynamics.
This section is based on [2].

1.5 Mathematical description of dissipative structures via Order Parameter Equations (OPES)

The mathematical expression of the similar behaviour is of special interest from theoretical point of view since beneath every structure lies a mathematical model.
The question is then: How can the similar behavior of all those very different systems showing spontaneous pattern formation be expressed?

This is done by so called *order parameter equations* - in the short form OPEs.

Those are equations of universal character which in their most general form are derived from basic assumptions like symmetries of the system. For a particular system the general expression gets adapted.

The OPE describes the spatio-temporal evolution of the system´s order parameter. The order parameter is the system state vector. This can be the electric field in a laser or the concentration in a chemical reaction e.g..

Sometimes the OPE for a system can be derived simplifying the microscopic equations of the system. Thus there´s a lot of systems that can be described by the same OPE adjusting the parameters in each case to obtain the equation for a system in particular.

The big fortitude of the order paramter equations is, that they describe a collectivity of phenomenons that appear in a system. Finding a common OPE is a big advantage in the case of a system that is difficult to investigate for technical reasons. The characteristics of this system can then be studied in a system that´s described by the same OPE but can experimentally be accessed much easier.

System properties get reflected directly in the kind of OPE describing them. Their solutions can qualitatively be very different. This suggests a classification of systems concerning the types of OPEs.

Most pattern forming systems in nature or physics can be described by Swift-Hohenberg (SHE) or Ginzburg-Landau (GLE) equation types.
They are universal equations that describe parametric processes in nonlinear self-oscillating spatially extended systems close to generation treshold.

The concrete form of the describing OPE for a particular system depends decisively on the symmetry and the tuning of the system.

The tuning paramter measures how far from the main resonance the self-oscillating system is excited.
The tuning of the system has influence on the character of the patterns displayed by the system and usually a system represents only a particular value of the detuning parameter. Optical systems constitute the general case, as they permit to work at arbitrary detuning values [3]. Under certain conditions (section 2.2) the optical system is well described by the Swift-Hohenberg

equation (SHE) and represents the predicted patterns dependent on the detuning (see sections 1.7 and 1.8).

Furthermore the kind of defects observed in nonlinear dissipative systems is strongly related to the degrees of freedom of the phase of the system order parameter. Hence a differentiation between phase invariant and phase-locked systems is useful:

Phase invariant systems can be described by a field with arbitrary phase (the phase is free). This can be expressed by a complex order parameter. Prototypical models for systems with complex order parameter (complex system) are equations of the complex Swift-Hohenberg or Ginzburg-Landau type (furtheron called CSHE and CGLE).
The CSHE and its solutions are discussed in section 1.7.

Phase-locked systems can be described by an order parameter with a phase attracted to certain discrete values. Usually there is one or two allowed phase values. Phase locked systems that exhibit more than two possible phase values are not common.
The descrete number of phases makes the mathematical description effectively real (we talk of real systems and real order parameters). Prototypical models for real systems are equations of the real Swift-Hohenberg or Ginzburg-Landau type (furtheron called RSHE and RGLE).
OPEs for phase-locked systems and the kind of patterns that they display are presented in section 1.8.

For certain values of the system parameters the solutions to the OPEs are especially interesting. That´s when the system displays localized structures.
The OPEs mentioned above are strictly valid near generation treshold. The structures presented in this project are displayed by systems working close to treshold. Structures can appear far from treshhold as well, but the theoretical description has to be adapted then.

In section 1.6 basic types of localized structures are presented.

Typical localized structures of complex systems are vortices and extended patterns are ensembles of vortices and travelling waves (see section 1.7). Usually the patterns of complex systems display a high degree of disorder.

Typical localized structures of real systems are domain walls. Examples of extended patterns are stripes or labyrinths, hexagons, domain walls and dark ring solitons (see 1.8).
Dissipative systems with broken phase symmetry (real systems) exhibit the more structured patterns than complex systems.

This section is based on [2], [4] and [3].

1.6 Localized structures

Solutions to the OPES are can be of quite different character depending on the system parameters.
While extended patterns are spread over all (or a large part) of the whole area of a spatially extended system, localized structures occupy small regions marking a kind of defect within areas of uniform solution or defining transitions between areas of different properties. They can have very different properties, but most of them have the following characteristics in common:
They separate different stable solutions of the system, they are quite insensitive to noise and small external perturbations, they can be generated and deleted by appropriate manipulation of the system and they are not coherent, hence they can be manipulated independently without this having any influence on the neighbors.
Thus localized structures in optics are of technological interest for information processing.

As already pointed out before, dissipative systems show a larger variety of localized structures than conservative systems.
There are two especially important types of localized structures, namely vortices and solitons. In both conservative and non conservative (dissipative) systems there are vortices and solitons found, but they differ in their properties from each other. For example there´s certain types of solitons appearing in dissipative systems, while they don´t appear in conservative ones.

There are many examples of vortices and solitons found in nature, as indicated in section 1.3, but also in science the phenomena of the formation of solitons and vortices has been observed. For instance supra-conducting vortices in the magnetic flux cavity vortices and cavity solitons in optics (see figures 1.1, 1.6 and 1.7).

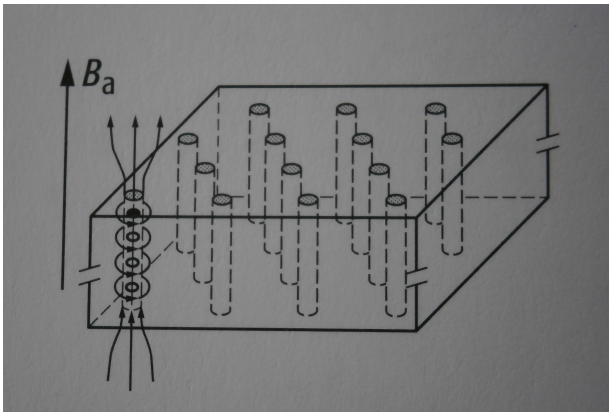

Figure 1.7: Magnetic flux quants - vortices in the magnetic flux (image taken from [20]).

In terms of mathematics vortices are local phase defects of the system order parameter.
On the site of the vortex the amplitude of the describing field is zero and the phase is singular. Around the vortex the order parameter phase varies continuously and accumulates a multiple of 2π along a closed loop [4].

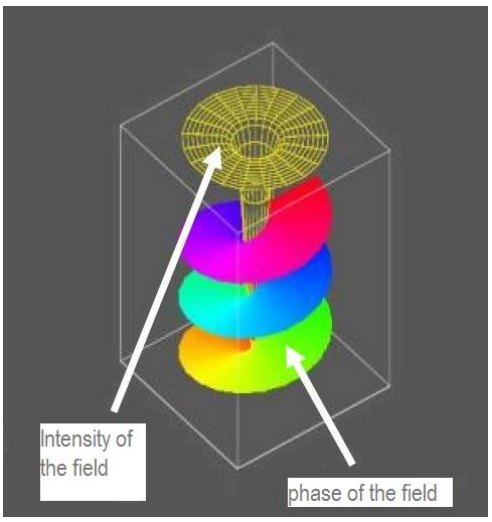

Figure 1.8: Scheme of a vortex. Image taken from [2].

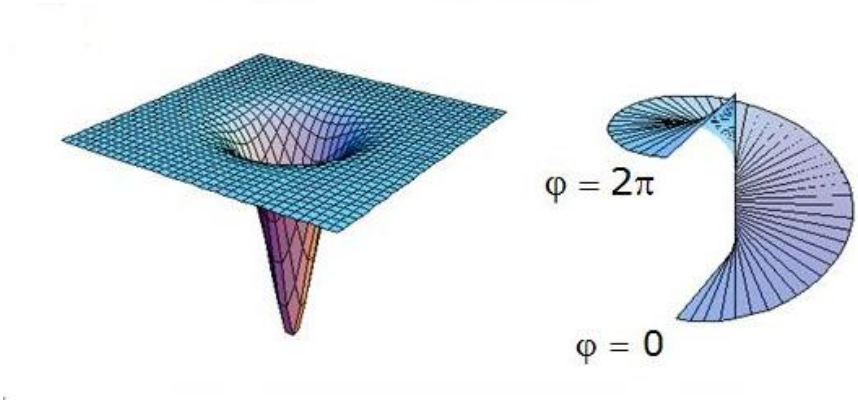

Figure 1.9: Alternative representation of a vortex. Image taken from [17].

Solitons are stable solutions of one-dimensional nonlinear wave equations. They show particle like behavior and that´s why they are called solitons.
Examples are kink-shaped solitons in water canals (see figure 1.1, image on the right) or form-stable electromagentic pulses. Such solitons find technological application in data transfer as they don't change their spatial, temporal or spatiotemporal shape (see figure 1.10). It should be mentioned that there has always been a big interest in localized structures of optical systems due to their potential applications in technology.

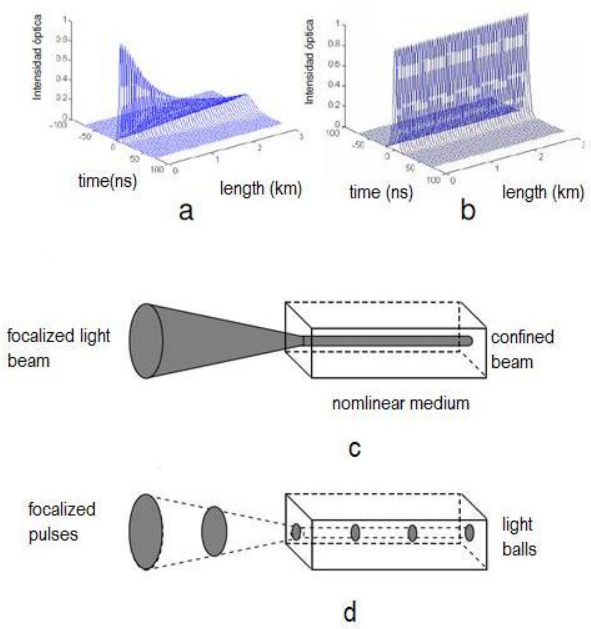

Figure 1.10: Examples of light solitions. A light pulse gets deformed by chromatic dispersion (a). In a nonlinear medium this can be compensated and temporal solitons formed (b). Schematic representation of a spatial (c) and a spatiotemporal soliton (d). Images taken from [2].

1.6.1 Vortices and solitons in optics

In optics both types of localized structures are found in nonlinear cavities.

Cavity vortices and cavity solitons are a particular type of localized structure.

They are formed in the transversal plane of the field confined in a resonator.
Cavity vortices appear in systems that are described by a complex order parameter, while cavity solitons appear in opctically bistable systems that are described a real order parameter. Figure 1.11 shows some examples of optical vortices.

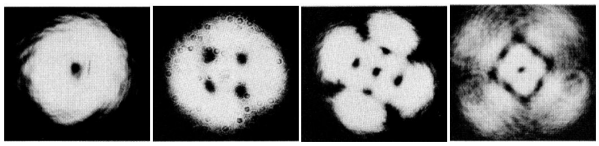

Figure 1.11: Experimental pictures of optical vortices in a resonator with Na_2 vapor (image taken from [2]).

Within the cavity solitons one can distinguish between phase and amplitude solitons (see figure 1.12).

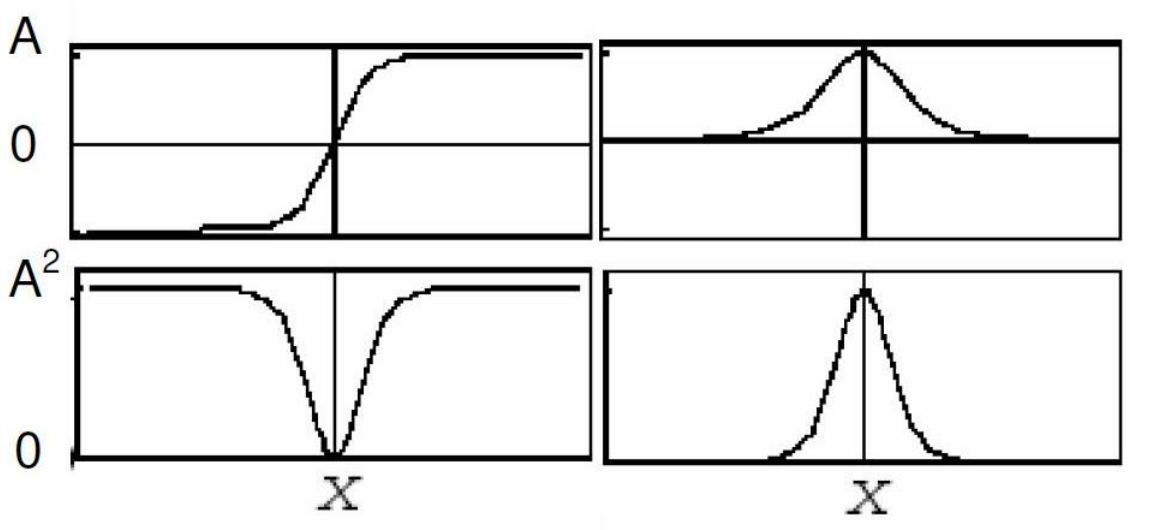

Figure 1.12: One-dimensional representation of a cavity phase soliton (left column) and amplitude soliton (right column). A is the field amplitude and X is the spatial coordinate. A phase soliton connects two states with the same amplitude and opposite phase. The amplitude soliton connects the same state going through an intermediate one. Image taken from [2].

Amplitude solitons can be brilliant or dark. The brilliant ones are observed on a dark background where the solitons appear as brilliant light dots. The dark ones appear as dark dots on a homogeneous illuminated background.

Phase solitons are stable structures that separate areas of equal field amplitudes but opposite phase (the phases differ in π radians).
Phase solitons can for example appear as dark lines that separate spatial domains of opposite phase or orthogonal polarization.
Alternative names for cavity phase solitons are dark line solitons, domain walls or simply phase solitons.

In nonlinear optical cavities phase solitons correspond to dark lines in the one dimensional case and to dark rings in the two dimensional case (see for example figures 1.29 and 1.31 respectively).

They can be considered a limiting case of a more general solution called domain wall.
A domain is a region in space of arbitrary size and form where the field with a certain phase and amplitude is separated from other regions with different phases and amplitudes.
A domain wall corresponds to the connection between two stable solutions (see figure 1.13).

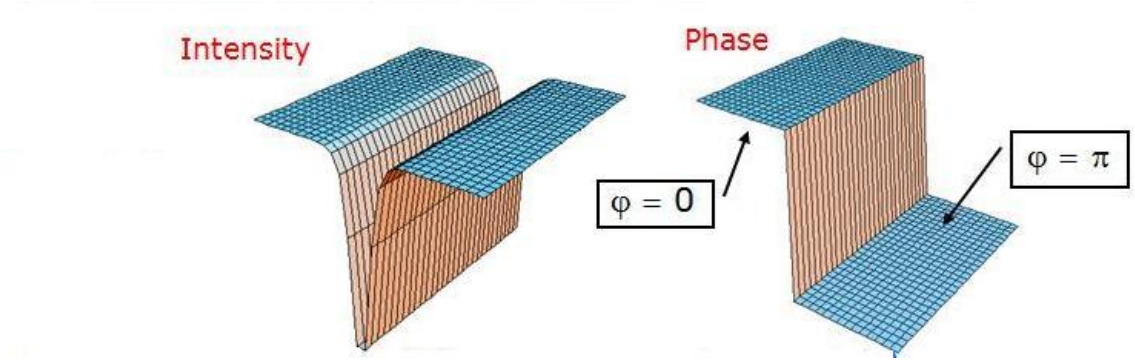

Figure 1.13: Schematic representation of a domain wall. Image taken from [17].

The existence of a particular localized structure is deeply related to the phase symmetry of the system and the character of the bifurcation between the trivial solution and the emission regime.

A supercritical bifurcation is characterized by the transition of the trivial to the oscillating solution varying continually the system control parameter and the two types of solution connect in the point of the bifurcation.
Examples of supercritical bifurcations are the supercritical Hopf and the supercritical Pitchfork bifurcation (see figures 1.14 a and c).

On the other hand a subcritical bifurcation is characterized by the existence of a finite difference that connects the trivial and the oscillating solution at the point of the bifurcation.
Further on both solutions can coexist beneath the point of the bifurcation, which originates bistability or hysteresis (see figure 1.14 b).

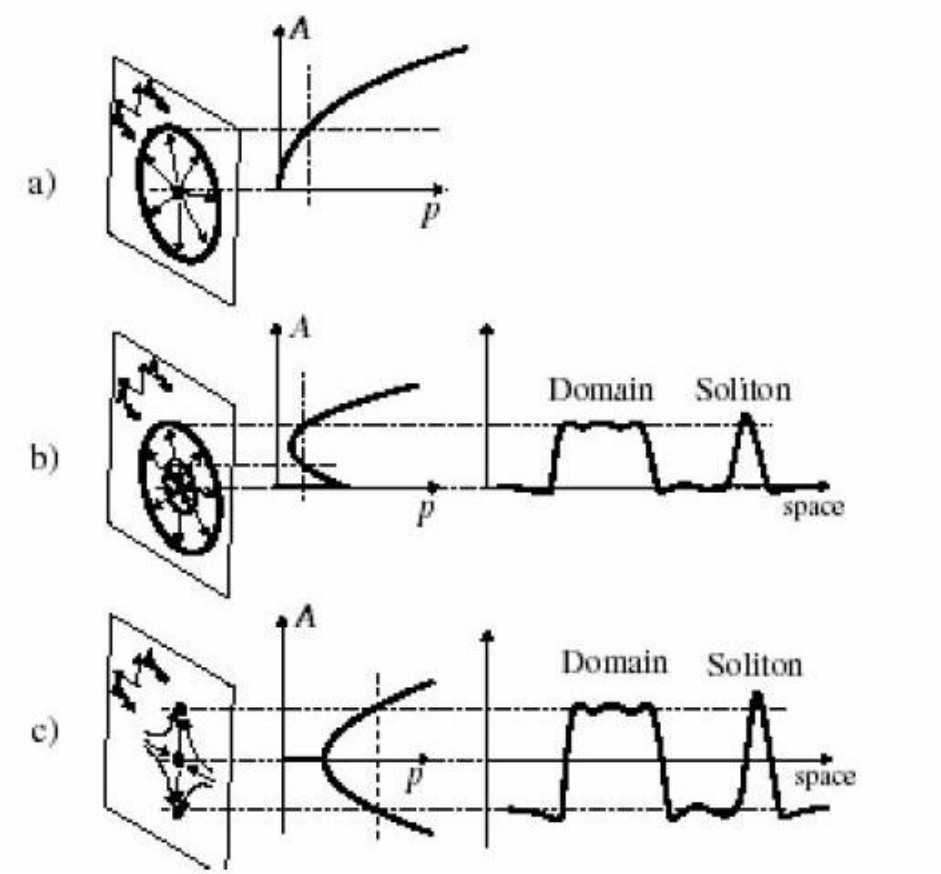

Figure 1.14: Different types of bifurcations in nonlinear systems and the type of structures supported by them. (a) Supercritical Hopf bifurcation, (b) subcritical Hopf bifurcation and (c) supercritical Pitchfork bifurcation. Image taken from [2].

Optical control of cavity solitons:
Amplitude cavity solitons have to be injected externally, while the phase solitons can be injected externally or appear spontaneously caused by noise. When this happens their spatial localization is arbitrary.
Once created those cavity solitons keep fixed in the same spatial position and can be deleted or displaced to another spatial position.

Vortices appear in systems that show phase invariance while they can´t be found in systems with broken phase symmetry.
Amplitude solitons appear in systems that show a subcritical bifurcation.
Phase solitons can appear in both, systems that show a subcritical and systems that show a supercritical bifurcation, as long as the system shows a rupture in the phase symmetry.
This section is based on [2].

1.7 Order parameter equations for phase invariant systems

The complex Swift-Hohenberg equation (CSHE) and the complex Ginzburg-Landau (CGLE) equation are appropriate equation types to describe the dynamics in phase invariant (complex) pattern forming systems.
The CSHE and CGLE describe self-oscillatory systems characterized by a homogeneous Hopf bifurcation. Such systems are paradigmatic for phase invariant systems, as the oscillating state reached after the bifurcation can have any phase. The model for this type of complex system can be generalized to other classes of complex systems and thus the discussion below is of general character. Examples are certain chemical reactions and several optical systems such as Optical parametric oscillators (OPOs) and lasers.
The equations in this section are written in terms of optics referring to the experimental realization. It has to be pointed out that nonlinear optics is capable of forming the whole variety of complex structures typical for general pattern forming systems [3].
In optics the CSHE describes pattern formation in the mean field approximation in nonlinear optical cavities of high Fresnel number in the case of a single longitudinal and multi-transversal mode resonance. Appropriate optical system described by the CSHE are discussed in section 2).

Examples are laser like systems like class A and C lasers, photorefractive oscillators (PROs) in two wave mixing (see section 2.4.) configuration and non degenerate optical parametric oscillators (OPOs).

The spatiotemporal dynamics of the order parameter $A(\vec{r}, t)$, which is proportional to the optical field envelope, is given by:

$$\frac{\delta A}{\delta t} = pA - A\,|A|^2 + i(a\nabla^2 - \Delta)^2 A \tag{1.1}$$

a ..... diffraction coefficient
∇ ..... Laplacian
Δ ..... detuning parameter
p ..... pump parameter, p « 1 is assumed (that´s close to oscillation treshold) so that the cubic approximation of the nonlinear term is justified.

Solutions to the Complex Swift Hohenberg equation:

Vortices, shocks, domains of tilted waves and cross roll patterns are typical patterns of the CSHE.
In what follows the different types of solutions (localized structures and extended patterns) to the CSHE dependent on the cavity detuning are discussed.

The detuning parameter is given by $\Delta = \omega_L - \omega_C$ with ω_L, ω_C being the lasing frequency and the frequency of the next nearest resonant cavity mode respectively.
All patterns are dynamic both in the numerical simulations and in the experimental observation.

$\Delta \leq 0$*:*
For zero or negative detuning the CSHE becomes the complex Ginzburg-Landau equation (CGLE), which can be obtained simplifying the laser type A equations.

$$\frac{\delta A}{\delta t} = pA - A\,|A|^2 + i(a\nabla^2 - \Delta)A \tag{1.2}$$

The waves with zero transverse wave-number are most strongly amplified and there is emission parallel to the optical axis of the resonator (see section 2). Characteristic patterns are vortices or spiral waves separated by shocks. Shocks are caused by counter propagating energy flows and appear between neighboring vortices.
Figure (1.15) shows numerical simulations and the experimental realization of the CHSE in the case of zero detuning.
The experiments were done in a high Fresnel number photorefractive oscillator with $BaTiO_3$ as active medium.
The range of zero or negative detuning is characteristic for chemical or biological pattern forming systems. Thus vortices can be found in those systems as well.

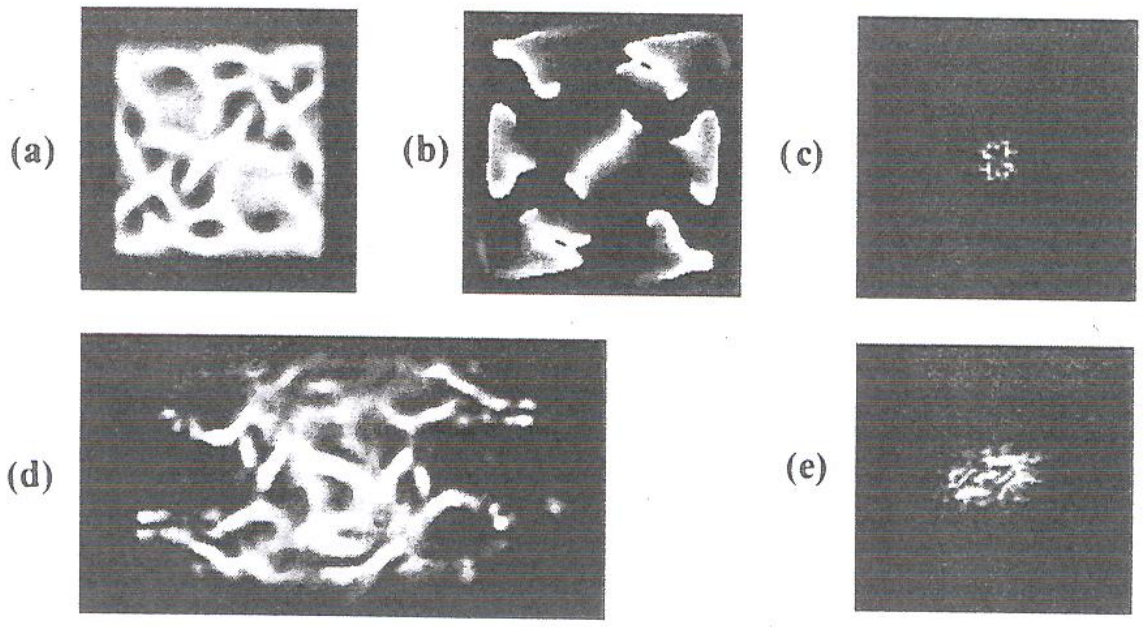

Figure 1.15: Numeric simulation [(a)-(c)] and experimental realization [(d)-(e)] of the CSHE for zero detuning. Vortices separated by shocks are observed. Near field: (a) and (d) amplitude, (b) phase. Far field: (c) and (e), both showing the amplitude. Image taken from [3].

$\Delta > 0$*:*
For positive detuning the patterns are qualitatively different:
So called Turing structures with nonzero transverse wave number components are most favored. In this case there is emission out of axis. A cone of modes with the same transverse wave number is excited (see section 2 figure (2.2).
The radius of the cone (the module of the transverse wave vector) is proportional to the detuning $|k\perp|^2 = \Delta$. The excited modes correspond to a resonant ring in the Fourier plane. The ring has

a finite width proportional to the gain line width $\Delta\omega$.

The basic characteristic patterns are tilted waves if no lateral boundaries are present. In this case only one transverse wave number from the resonant ring wins the nonlinear competition and determines the pattern (see section 2, figure (2.2)).

Influences of the boundaries get reflected in the pattern by the appearance of domains of differently oriented tilted waves. In each domain the field has a particular phase value. The boundary between two domains of tilted waves can contain vortices. At the site of the vortex the transition from one to the other phase is not defined, constituting a local phase defect.
Figure 1.16 shows numeric and experimental results for this case of positive detuning.

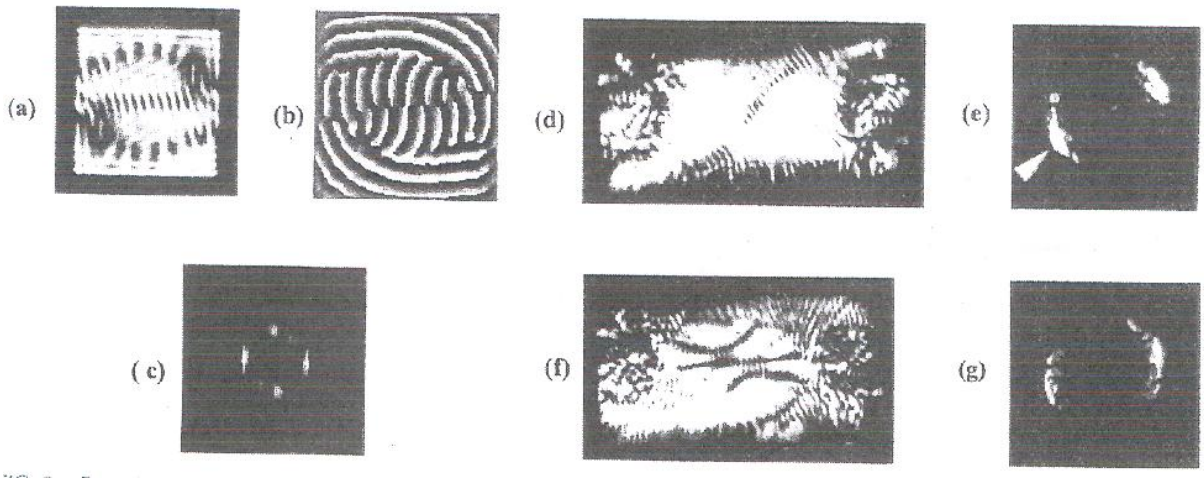

Figure 1.16: Numeric simulation [(a)-(c)] and experimental realization [(d)-(g)] of the CSHE for positive detuning. Domains of tilted waves separated by a row of vortices are observed. Near field: (a), (d) and (f) amplitude, (b) phase. Far field (c), (e) and (g). In (d) two domains of different tilt separated by vortices are visible, in (f) there is four.
Image taken from [3].

This section is based on [3].

1.8 Order parameter equations for phase locked systems

A large class of pattern forming systems in physics is described by real order parameter equations. But usually those systems represent a particular value of the detuning parameter. Optical systems constitute the general case, as they permit to work at arbitrary detuning values. Therefore the results discussed in the following are characteristic not only for optics, but the equations are written in terms of optics.

Within the phase locked systems there´s distinguished between systems where the order parameter has a constant phase (e.g. the laser with injected signal), systems which are bistable in phase (e.g. degenerate optical parametric oscillators (DOPOs),photorefractive oscillators (PROs) in degenerate four wave mixing configuration (see 2.4.2)), and such with more than two possible phase values (they exist, but are very rare).

Systems locked to a single phase:

The locking of the system to a fixed phase value can be achieved by parametric forcing on a 1:1 resonance of a complex system described by the forced CGLE (1.8). A paradigmatic example is the laser with injected signal, where the arbitrary phase of the free running laser gets locked to the phase of the injection.
It can be described by:

$$\frac{dA}{dt} = 4(1 + i\Delta)Y + pA - A|A|^2 - 4a\nabla A - \frac{4}{3}a^2\nabla^2 A \tag{1.3}$$

Where Y is an external injection, p is the pump parameter, Δ is the detuning between the eigen frequency of the system and the frequency of the injection.

Systems showing bistability in phase:

They can be described by the real Swift-Hohenberg equation (RSHE) or the real Ginzburg-Landau equation (RGLE). The real Swift-Hohenberg and Ginzburg-Landau equations are universal models for phase bistable systems. In the case of lasers the GLE describes the single mode two - level lasers with bichromatic injection close to threshold of the free running laser.

The RSHE reads:

$$\frac{dA}{dt} = pA - A^3 + (a\nabla^2 - \Delta)^2 A \tag{1.4}$$

Where $A(\vec{r}, t)$ is real valued. It is defined in 2D space $\vec{r} = (x, y)$ and evolving in time.
a..... diffraction coefficient
∇..... Laplacian
Δ..... detuning parameter
p..... pump parameter, $p << 1$ is assumed (that´s close to oscillation treshold) so that the cubic approximation of the nonlinear term is justified.

A paradigm for a bistable system is the degenerate optical parametric oscillator (DOPO).
The RSHE for the particular case of the DOPO and the solutions to this equation are discussed below.
Due to the general character of the RSHE the results of its´ analyze can also be applied to other systems like degenerate four wave mixing (DFWM) in resonators of high Fresnel number.

Phase bistability can also be induced into some initially phase invariant systems by external actions. The classical way is parametric forcing at double its natural frequency (section 1.9).
Such kind of external forcing is described by the Ginzburg-Landau equation with parametric pumping given by eq.(1.9).

Alternatively phase bistability can be introduced by Rocking (sections 1.9.2 and 1.9.3) and is described by equations (1.13) or (1.17), which are similar to eq.(1.9).

Solutions to the Real Swift Hohenberg equation on the example of the DOPO:

In what follows the different types of solutions (localized structures and extended patterns) to the RSHE dependent on the cavity detuning are discussed.

The RSHE adapted to the case of a DOPO is given by:

$$\frac{dA}{dt} = A - A^3 + (\nabla^2 - \Delta)^2 A \tag{1.5}$$

The parameters are as described above for equation (1.4).
The detuning parameter is given by $\Delta = \omega_P - \omega_C$ with ω_P and ω_C being the pump wave frequency and the frequency of the closest resoant cavity mode respectively.
Equation (1.5) is valid for zero or small detuning and close to oscillation threshold.

The structure formation is based on a phase bistability.
Localized structures are domain walls. In spatially extended systems fronts separating domains of opposite phase (differing by π) are found. Extended patterns are Turing patterns (stripe patterns), hexagons, rolls and phase domains. The dynamics depend on the resonator detuning, fronts expand or shrink.
For certain parameter values there are stable structures formed, that´s spatial solitons.

Positive detuning ($\Delta > 0$):

For large positive detuning $\Delta >> 0$, equation (1.5) predicts Turing patterns.
For example stripes

$$A(\vec{r}) \propto cos(\vec{k} \cdot \vec{r}) \tag{1.6}$$

with a resonant wave number $|\vec{k}| = \sqrt{\Delta}$.
This range of detuning is what describes e.g. Rayleigh-Bernard convection, where the convection cells have a defined size.

Zero detuning ($\Delta = 0$):

In the limit of zero detuning $\Delta \cong 0$ the RSHE describes parametrically excited systems. In this case two solutions with homogenous amplitude and phases $\phi_0 = 0$ or π are characteristic. In spatially extended systems one region can take one phase and the rest takes the opposite phase. Between the two domains of opposite phase a dark line appears, because the amplitude of the field is zero.

Dynamics:
The dynamics of the patterns depend on both the curvature and the detuning. For small detuning the homogenous states are preferred. Domains shrink and finally disappear (see fig. 1.17 b).

For large detuning existing domains expand until there is a labyrinth structure formed that fills all the area (see fig. 1.17 a). The labyrinth is a Turing structure, it can be considered as a stripe pattern with defects.
For even larger values of detuning the homogenous solutions become modulationally unstable. New domains nucleate and expand. The pattern becomes more and more the stripe pattern mentioned above.

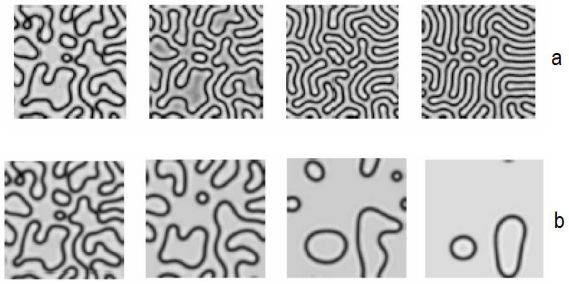

Figure 1.17: Evolution of phase structures following the RSHE:
a) Expansion of domain boundaries until labyrinth structures are developed in the case of large detuning, b) Contraction of domain boundaries in the case of small detuning. Image taken from [2].

For intermediate values of detuning, but within the range of shrinking domains, the shrinking can stop at a particular domain size and doesn´t shrink until it disappears. This happens when the contraction is compensated by the repelling of the domain walls. A stable circular domain with finite radius is formed called dark ring soliton (see fig.1.18). The phase inside the ring is opposed to the phase outside the ring and the circle connecting those two regions of opposite phase is a ring of zero amplitude.

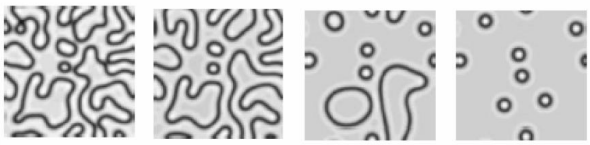

Figure 1.18: Formation of phase solitons (dark ring solitons) for intermediate values of detuning in the RSHE. Image taken from [2].

Experimentally the numeric results are confirmed.
An experiment was realized by degenerate four wave mixing in a near-self-imaging resonator, using BaTiO3 as nonlinear material. The gain was moderately above threshold, in order to realize the results of the RSHE discussed above.
In the experiment only the detuning parameter was varied, the other parameters were kept constant.
The detuning parameter was chosen by the variation of the resonator length on an optical wavelength scale.
The behavior of the pattern dynamics numerically found was also experimentally observed.
Figure 1.19 corresponds to figure 1.17 b and shows the dynamics for small detuning.

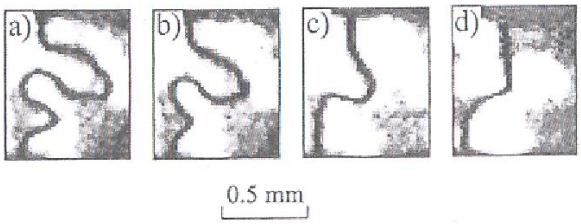

Figure 1.19: The shrinking of a domain boundary for almost zero detuning observed in time steps of 2 sec in a PRO. Image taken from [5].

Figure 1.20 corresponds to figure 1.17 a and shows the dynamics for small detuning.

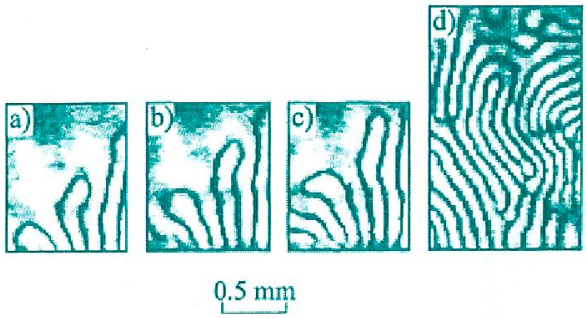

Figure 1.20: The expansion of domain boundaries and the final formation of a labyrinth structure for large positive detuning in a PRO. Image taken from [5].

Also the stable structures called dark ring solitons found for intermediate values of detuning were experimentally found. Figure 1.21 corresponds to figure 1.18.

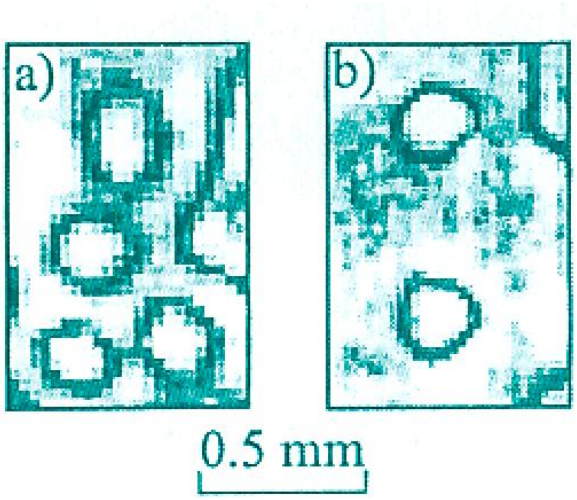

Figure 1.21: Formation of phase solitons in a PRO. a) shrinking domains , b) stable localized structures. Image taken from [5].

This section is based on [2] and [5].

1.9 Conversion of a complex into a real system

In this section, mechanisms to break the phase invariance of phase invariant systems will be presented.
As mentioned in the sections above, the type of localized structures supported by extended nonlinear systems is strongly related to the symmetry properties of the system.
The localized structures displayed in a phase invariant systems described by the CSHE or CGLE are vortices. Typical extended patterns are ensembles of vortices and travelling waves usually displaying a high degree of disorder (see section 1.7).
On the other hand there are domain walls (see section 1.8) supported by phase locked systems. The domain walls decay in arrays of vortices in complex systems.
Especially the patterns of bistable system tend to be quite structurefull, e.g. stripes or labyrinths, hexagons, domains and dark ring solitons (see section 1.8).

From technological and fundamental point of few the patterns formed in dissipative systems with broken phase symmetry (real systems) are the more interesting ones than the ones of phase invariant (complex) systems. Especially bistable systems exhibit structurefull patterns.

On the other hand there is interest in avoiding the spontaneous formation of vortices by the external control of self-oscillatory spatially extended nonlinear systems, because the spontaneous emergence of vortices cause turbulences [1].

Self-oscillatory systems characterized by a Hopf bifurcation are paradigm for phase invariant systems, as the oscillating state reached after the bifurcation can have any phase. They show a spontaneous transition between a stationary and an oscillatory state, both spatially homogenous.

Several examples for such systems are given in optics. For example lasers, non degenerate optical parametric oscillators (OPOs) and photorefractive oscillators (PROs) in non degenerate wave mixing configuration.
There are also non optical systems presenting phase invariant self-oscillation. For example certain chemical reactions.
The mechanisms presented here consider this paradigmatic example of a complex system but can be generalized to other classes of complex systems.
This section is based on [4], [6], [7] and [2].

1.9.1 Phase locking via Parametric forcing

Parametric forcing is the classical way to break the phase invariance in nonlinear oscillators. It consists in driving the system periodically in time.

There are nonlinear oscillating dissipative systems that, when forced externally by a periodic force show a resonant response, when the ratio between the frequency of the external forcing and the natural frequency is close to $n : m$, n and m being integers and $n > m$.
Such systems respond with their natural frequency (or close to) but adjust the phase of the describing order parameter in a way, that is determined by the forcing.

This characteristic of oscillating systems allows in the special case of forcing with double the natural frequency of the system that there are two possible states with amplitudes taking each a defined phase value (one differing from the other by π radians).
The effectiveness of the parametric forcing mechanism is given by the Arnol´d tongues shown in figure 1.22.

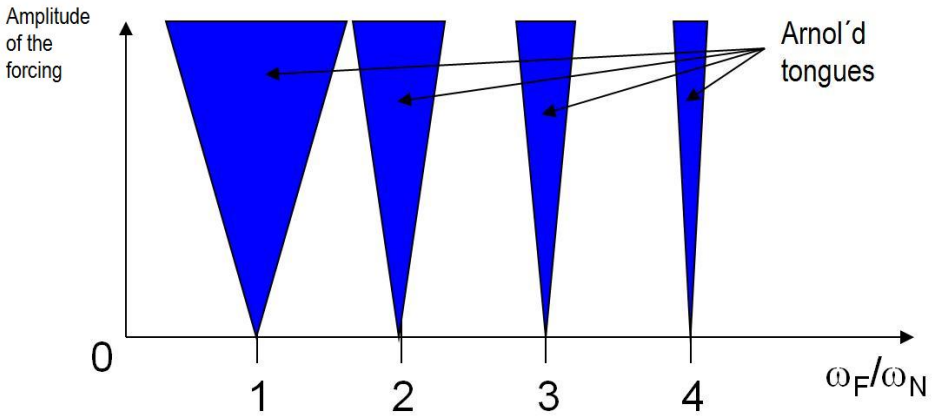

Figure 1.22: Effectiveness of the parametric forcing mechanism. Within the blue regions the oscillations are frequency locked. Image taken from [17].

The ratio of the frequency also determines the number of phase values that the system can lock to.
There is n equivalent phases imposed when forcing on a $n : m$ resonance, given by
$\phi_k = \phi_1 + 2\pi(k-1)/n$, with $k = 1, \cdots, n$.
This can easily be understood by symmetry considerations. Figure 1.23 shows the case for $n = 2$, which is forcing at double the system´s natural frequency.
The system adjusts the phase of its order parameter to the one of the external forcing. There are two equivalent possibilities to do this differing by a phase shift of π radians. Hence the system can be considered as bistable in phase.

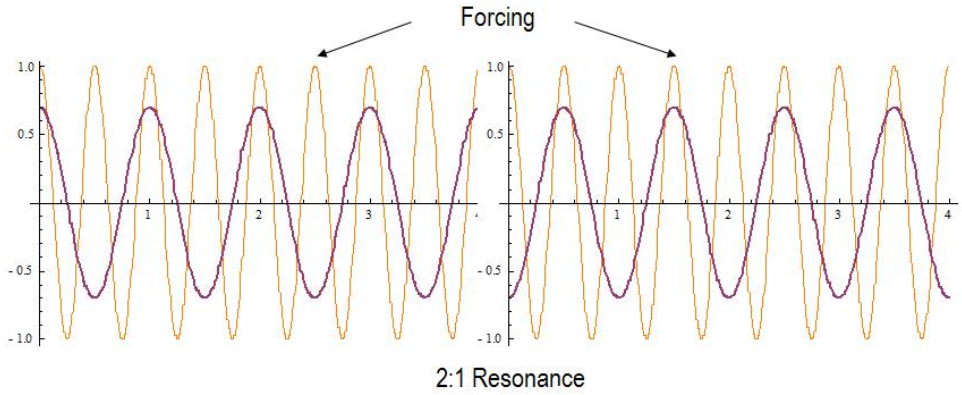

Figure 1.23: The system adjusts the frequency of oscillation (violet line) to the one of the external forcing (yellow line). The left and right side are equivalent situations. The system is thus bistable in phase. Image taken from [17].

Close to oscillation threshold, this kind of forcing can be described universally.
A $n:m$ resonance is defined by $\omega_e = (n/m)(\omega_0 + \nu)$.
Here ω_e is the external forcing frequency, ω_0 is the natural frequency of oscillations, n/m is an irreducible integer fraction and ν is a small detuning.

Under the slowly varying amplitude approximation the dynamics of the complex amplitude of oscillations A (the system order parameter) is given by:

$$\frac{dA}{dt} = (\mu + i\nu)A + (1 + i\alpha)\nabla^2 A + (1 + i\beta)A\,|A|^2 + F^m(A^*)^{n-1} \tag{1.7}$$

In eq. (1.7) all parameters are real and adimensional.
F is proportional to the amplitude of the forcing.

$\nabla^2 = \delta_x^2 + \delta_y^2$...when z is the direction of propagation
μ...excitation parameter (proportional to the increase of the control parameter from its value at the bifurcation).
ν... detuning parameter
β... nonlinear frequency shift coefficient
α... dispersion coefficient

This equation is a *parametrically forced complex Ginzburg-Landau equation (PGLE).*

$F = 0$:
In the absence of forcing this equation is the complex Ginzburg Landau equation (CGLE), which describes self-oscillatory systems close to threshold.
Examples are self-oscillatory chemical reactions and nonlinear optical cavities, such as lasers.
In these cases the electric field in the laser and the concentration in the chemical reaction are the order parameter of the system and can be written:

$Re(A(x, y, t)exp[-i(\omega_0 + \nu)t]$.

The unforced system is complex, as the solutions allow any phase value to the order parameter.
The type of localized defects described by the CGLE are vortices as described in section 1.7.
The CGLE is the complex Swift-Hohenberg equation (CSHE) for negative values of detuning.

$F = const.$, $n = m = 1$:
Parametric driving in a 1:1 resonance determines the frequency and stabilizes the phase of the oscillation. There is only one possible phase value that the order parameter can take, imposed by the external forcing.
This corresponds to a laser with externally injected signal.

$$\frac{dA}{dt} = (\mu + i\nu)A + (1 + i\alpha)\nabla^2 A - (1 + i\beta)A\,|A|^2 + F \tag{1.8}$$

The system adjusts its phase to the one of the external forcing F. The system is locked to one stable phase value.

To achieve two possible phase values, the system has to be driven in a 2:1 resonance. That´s forcing at double the natural frequency. Taking eq. (1.7) with

$F = const.$, $n = 2$, $m=1$:

$$\frac{dA}{dt} = (\mu + i\nu)A + (1 + i\alpha)\nabla^2 A + (1 + i\beta)A\,|A|^2 + FA^* \tag{1.9}$$

The last term implies a phase symmetry. Solutions a and $-a$ shifted by π radians in phase are equivalent. The system can adjust its phase in two equivalent ways to the one of the external forcing. Thus the systems is bistable in phase.

Not all systems can be modified by a forcing at double their natural frequency. Many systems don't respond to a forcing at a frequency much different from their natural resonance.

A famous example is the laser. As the laser has a small gain curve, it can only be excited within a small range around the laser emission level.
In this case the only possibility is forcing with or close to the system´s main resonance.
Parametric forcing is limited to the 1:1 resonance and therefore only locking to one single phase value can be achieved by this technique.

The question is if there a possibility to lock a system to two phases instead of only one forcing it at or close to its natural frequency?

The answer is found by the *Rocking* technique. Rocking is a versatile instrument to convert a phase invariant system into phase locked system with two defined phase values. As it works on the main resonance of a system its application is universal.

There has to be distinguished between temporal Rocking and spatial Rocking. Temporal Rocking was published in [4]. It has already been experimentally realized [6].

The experimental realization of the spatial Rocking, published in [1], was issue of this master´s project.

Rocking basically consists in the forcing at a frequency close to the system´s natural one while the amplitude of the applied force is modulated in time (temporal Rocking) or space (spatial Rocking). This is a generalization of the parametric forcing on a 1:1 resonance to the bichromatic case.

The two forms of Rocking, spatial and temporal, are supposed to equivalently cause a symmetry-break in phase invariant systems, so that the system gets locked to two defined phase values.
In the following sections the two Rocking techniques will be explained in more detail.

1.9.2 Temporal Rocking

"The idea is to drive the system with a spatially uniform, amplitude modulated forcing almost in resonance with the natural frequency of oscillations, which is a generalization of the classical periodic forcing in a 1:1 resonance to a quasiperiodic case, [4]."

There is a forcing considered, whose amplitude is slowly modulated in time: $F = F_0 cos(\Omega t)$.

This is actually a two frequency forcing as the actual forcing consist of the two frequencies $\omega_e \pm \Omega$.
The dynamics in then governed by eq. (1.8) with $F = F_0 cos(\Omega t)$ and reads

$$\frac{dA}{dt} = (\sigma + i\nu)A + (1 + i\alpha)\nabla^2 A - (1 + i\beta)A\,|A|^2 + F cos(\omega t) \tag{1.10}$$

$F = F_0/|\mu|$ is taken as real and positive, without loss of generality
$\omega = \Omega/|\mu|$
$\nabla^2 = \delta_x^2 + \delta_y^2$...when z is the direction of propagation
$\sigma = sgn(\mu)$
μ...excitation parameter, proportional to the increase of the control parameter from its value at the bifurcation
ν... detuning parameter
β... nonlinear frequency shift coefficient
α... dispersion coefficient

Pictorial picture - variational case:

To visualize the effect of the temporal Rocking, the simple case of a spatially uniform order parameter and $\alpha = \beta = \nu = 0$ (zero dispersion, zero diffraction, zero detuning) is considered.

This is the so called *variational* case, since eq.(1.10) can be written:

$dA/dt = -\delta V/\delta A^*$,

with corresponding potential

$$V = -\sigma|A|^2 + \frac{1}{2}|A|^4 - 2F cos(\omega t) ReA \tag{1.11}$$

The discussion of the form of this potential concerning the kind of forcing gives a pictorial picture of the Rocking mechanism. The phase locking mechanism can be interpreted as a result

of the periodic rocking of the system potential.

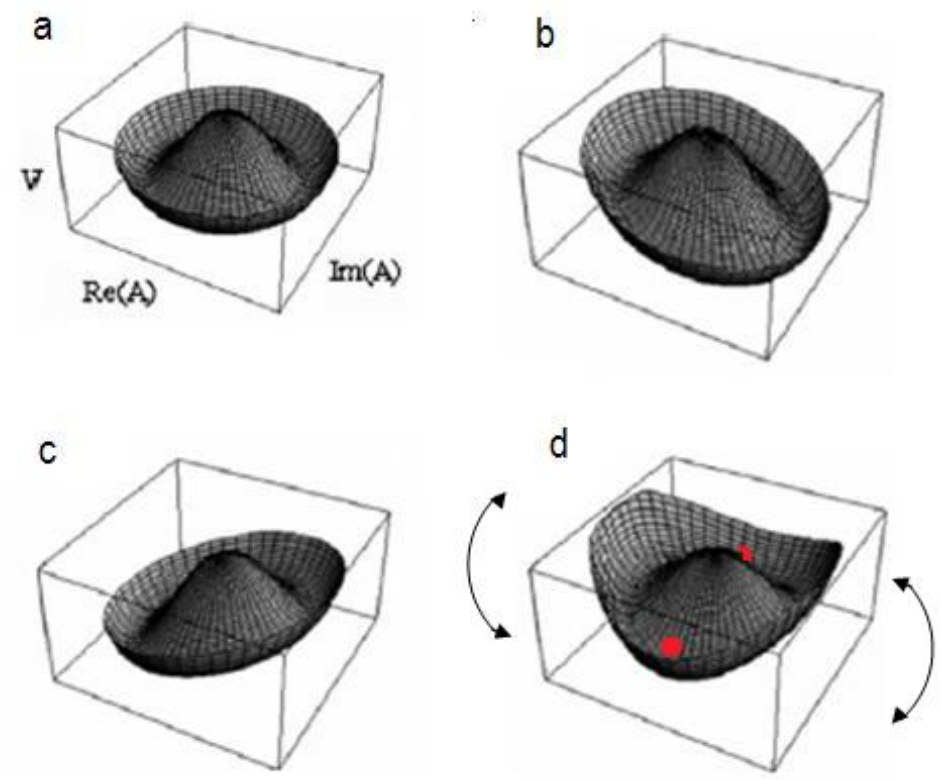

Figure 1.24: Schematic representation of the potential eq.(1.11) associated with eq. (1.10) in arbitrary units. (a) $F = 0$, no forcing is applied. The potential is radially symmetric and the order parameter´s phase is undetermined. (b) and (c): $F = const.$ and $\omega = 0$, constant forcing at the system´s oscillation frequency. The potential gets tilted proportionally to the forcing amplitude. In b) $F < 0$ and in c) $F > 0$. (d) $F = const.$ and $\omega \neq 0$. Rocking is applied leading to the periodic tilting of the potential around the axis ImA. The red dots mark the two equivalent positions that the order parameter prefers. Image taken from [7] with symbols added in (d).

In the case of $F = 0$:

In the absence of forcing the potential is isotropic on the plane of the complex order parameter $A = (ReA, ImA)$.

For $\sigma = -1$, that´s beneath oscillation threshold, the potential is minimum at the origin of the imaginary plane (figure 1.25 left column).
This corresponds to solutions with zero amplitude of the order parameter.

For $\sigma = +1$ (above threshold), the potential exhibits a local maximum at the position with $A = 0$ and a degenerate minimum along a circle with $|A|^2 = 1$.
It has the shape of a sombrero ((fig. 1.25 left column and fig. 1.24 a). The origin now corre-

sponds to an unstable trivial state of the order parameter $A = 0$ and the circle corresponds to the spatially uniform steady state with arbitrary phase.

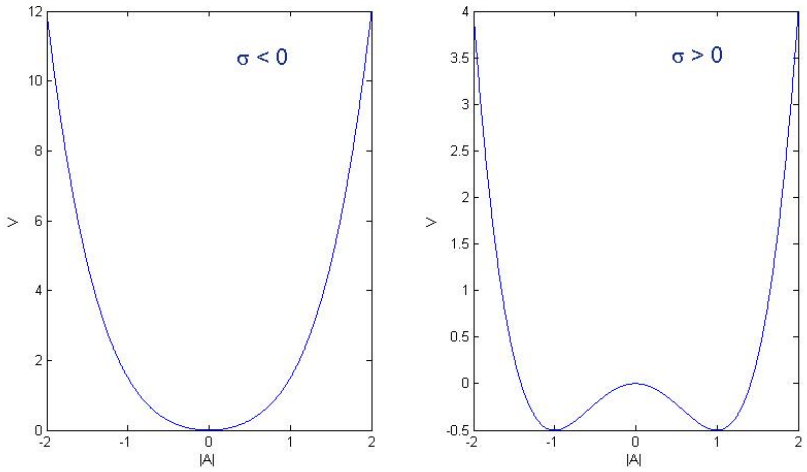

Figure 1.25: Schematic representation of the potential eq. (1.11) beneath ($\sigma < 0$) and above ($\sigma > 0$) oscillation treshold.

For $F = const.$ and $\omega = 0$:
This is the case of the classical driving in 1:1 resonance. The potential gets tilted along the axis ReA and the potential displays an isolated minimum on the axis ReA (fig. 1.24 b and c).

This implies the rupture of the system´s phase invariance. The order parameter $A = (ReA, ImA)$ gets locked to the position of minimum potential and takes a phase 0 or π with respect to the phase of the external force.

For $F = const.$ and $\omega \neq 0$:
For a periodic forcing term the potential V gets tilted periodically (rocked) around the axis ImA. Hence this kind of forcing is called Rocking.
The former positions of minimum potential on the axis ReA are now converted in sites of maximum change in potential. The potential at these points now alters between minimum and maximum values with the modulation frequency ω of the rocking.
Above oscillation threshold ($\sigma = +1$) the origin is repulsive since the potential exhibits a local maximum. The order parameter avoids in principle this point and follows two equal trajectories (differing in the sign of ImA) to reach the position of minimum potential.

Simulations show that for moderate modulation frequencies ω of the rocking the order parameter follows the position of minimum potential oscillating back and forth crossing the axis ImA.
In the limit of fast rocking ($\omega >> 1$) the order parameter doesn´t follow the periodic tilting of the potential any more. Areas where the potential is very dynamic are considered "noisy" and according to general principles of physics (reference [3] of [7]) the system state prefers phase

values that correspond to "quiet" areas in phase space.
In the present example the quiet areas are located on the imaginary axis. Thus instead of following two possible trajectories (crossing the positive or negative axis ImA) the order parameter locks to either of the two phase values π or $-\pi$ situated on the axis ImA (fig. 1.24 d).
The two phase values introduced by the rocking don´t have to be π or $-\pi$ but they differ in π and are symmetric with respect to the phase value of the injection.

In mathematical terms Rocking causes the transformation of the radial symmetric Hopf-Bifurcation describing the self-oscillatory system without forcing into a pitchfork bifurcation (see figure 1.14).

The pictorial picture given above is an intuitive way to explain how the conversion of an initially phase invariant into a bistable system via temporal rocking works, but as shown below this picture still holds even in the more general nonvariational case.
It is important to mention, that the phase locking mechanism via rocking doesn´t work only for high frequencies as it could be supposed by the picture given above. But one can say that the mechanism is effective in a 'Rocking window´, that´s defines a regime for the system parameters, where rocking works. It is particular for each system. This Rocking window is discussed for the case of a type A laser in [7] and a photorefractive cavity in [6].

In any case Rocking doesn´t work beneath oscillation threshold (see the following analytical discussion). In the pictorial picture presented here this can be explained by form of the potential. For $\sigma = -1$ the local maximum of the potential vanishes and the origin with zero amplitude of the order parameter becomes a stable solution.

General treatment - nonvariational case:

In the more general case with non zero values for the parameters ($\alpha \neq 0, \beta \neq 0, \nu \neq 0$) the mechanism explained for the simple case with $\alpha = \beta = \nu = 0$ still works.

For the analytical discussion the limit of strong and fast rocking ($F = O(\omega)$, $\omega >> 1$) is considered. At the end of the analytic discussion numeric simulations for a rocking frequency ω not much larger than one will be presented, showing that the mechanism is not limited to large frequencies for being effective.

In the considered limit of strong and fast rocking it is possible to separate the slow time scale t from the unforced system from the fast time scale $\tau = \omega t$ of the rocking. Further it is possible to seek solutions to eq.(1.10) in series of ω of the form $A(x, y, t) = A_0(x, y, t, \tau) + O(\omega^{-1})$.

At order ω the first term, $A_0(x, y, t, \tau)$, turns out to split into a sinus depending on the fast time scale constituting the real part and an imaginary part depending on the slow time scale:

$$A_0(x, y, t, \tau) \propto sin(\tau) + ia(x, y, t) \tag{1.12}$$

The evolution equation for $a(x, y, t)$ is found as solvability condition at order ω^0:

$$\frac{\delta a}{\delta t} = (\lambda + i\theta)a + (1 + i\alpha)\nabla^2 a - (1 + i\beta)|a|^2 a + \gamma(1 + i\beta)a^* \tag{1.13}$$

This equation is a CGLE (eq. (1.7) with $F = 0$) with an additional term containing the complex conjugate of a, making the gain phase sensitive.

The parameters are functions of the parameters in eq. (1.7) (for details see [4]).

$\gamma = \frac{1}{2}(F/\omega)^2$ is called the rocking parameter.

Looking at the eq. (1.9), which describes the classical way to introduce bistability (parametric forcing in a 2:1 resonance), one notes the similarity to the result of Rocking.

As eq. (1.9) also eq. (1.13) imposes the phase symmetry $a \to -a$.
Hence solutions with phases differing by π radians, a and $a \cdot e^{i\pi}$, are equivalent. The system can lock to either one of those two states, being thus bistable.
Both equations can be described by an effective real order parameter, since apart from a constant phase, the solutions are $|a|$ and $-|a|$.

Hence Rocking causes the conversion of a former complex system into an effective real one.
Such a rocked system should exhibit the same kind of localized structures as appearing in systems which are described by a real order parameter.

Figure 1.26 shows numeric simulations for the case with and without Rocking.
Without Rocking the system exhibits the type of patterns typical for complex systems, described in section 1.7. When Rocking is applied typical structures of real systems appear (see section 1.8).

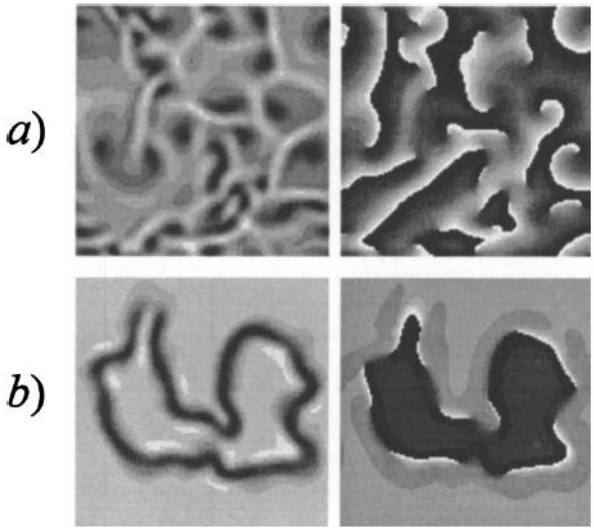

Figure 1.26: The patterns of complex systems are converted into such of real systems under the action of Rocking. Numeric integration of a) the CGLE (eq.(1.7) for $F = 0$) and b) the GLE with Rocking (eq.(1.10)). Left column: amplitude, right column: phase. Image taken from [4].

Discussion of the solutions to equation (1.13), which is the evolution equation of $a(x, y, t)$:

Apart from the trivial solution $a = 0$ there are two relevant spatially homogenous solutions to eq. (1.13), given by:

$a = \pm|a| \cdot e^{i\phi}$

$|a|$ depends on the excitation parameter μ, the rocking parameter γ and the detuning ν.

For $\sigma = -1$ (below threshold), the dependance of the amplitude on the parameters implicates $|a|^2 < 0$. Thus rocking works only above threshold (in the regime of self-oscillation, i.e. above the bifurcation).
The physical requirement of $|a|^2 > 0$ leads also to a restriction for the detuning parameter $\nu^2 < 1/3$.

Further conditions for rocking being effective are derived from a linear stability analysis of both the trivial and the rocked states against spatial modulations of the wave number k. This instability can be induced by detuning the system and depends furthermore on α and γ.

For $\alpha\nu \leq 0$ the system is bistable, while for $\alpha\nu > 0$ the two oppositely phased spatially homogenous rocked states become unstable.
Hence for $\alpha\nu \leq 0$ the system can exhibit domain walls connecting the two oppositely phased rocked states.

One-dimensional solutions: Ising and Bloch walls

For the simple case of one spatial dimension and $\alpha = \beta = \nu = 0$ (variational case) there exist analytical solutions to Eq. 1.13 above threshold. They are known as Ising and Bloch walls.

The Ising wall is given by:

$$a_I(x) = \pm g \cdot tanh(gx/\sqrt{2}) \tag{1.14}$$

And the Bloch wall is given by:

$$a_B(x) = \pm[g \cdot tanh(\sqrt{2\gamma}x) \pm i\sqrt{1-5\gamma} \cdot sech(\sqrt{2\gamma}x)] \tag{1.15}$$

Where $g = \sqrt{1-\gamma}$ and γ is the rocking parameter $\gamma = \frac{1}{2}(F/\omega)^2$.

The Ising wall shows up as a dark line and the Bloch wall as a grey line (see figure 1.27).

In the case of the Ising wall the field intensity at the interphase is zero and the phase changes apruptly. In the case of a Bloch wall the field intensity at the interphase is non zero and the phase changes continously.

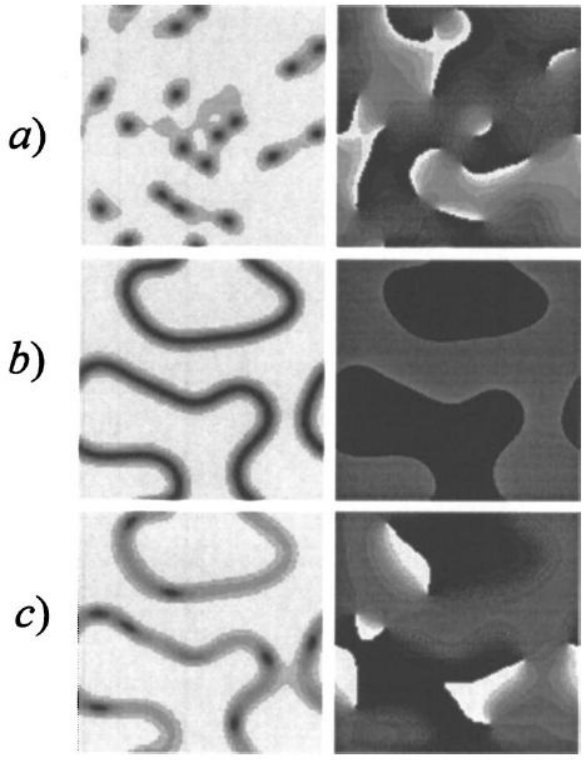

Figure 1.27: Numeric integration of the ac-driven CGLE (eq. 1.10) in the variational case. Intensity (left column) and phase (right column) of A, averaged over one Rocking period. Without driving, F = 0, vortices are observed (a). With Rocking, $\Omega = 4\pi$, phase domains separated by Ising walls (b) or Bloch walls (c) appear for strong and weaker Rocking respectively. Image taken from [4].

The stability of these two solutions depends on the rocking parameter $\gamma = \frac{1}{2}(F/\omega)^2$.

Ising walls are stable for a rocking parameter $1/5 < \gamma < 1$, Bloch walls are stable for $0 < \gamma < 1/5$. For $\gamma = 1/5$ a transition between the two of them takes place.

Hence for strong forcing the Ising walls are stable. They indicate a sharp transition between regions of opposite phase. The order parameter vanishes at the interface and the interface thus appears as a dark line.
For weaker forcing Ising walls turn into Bloch walls. The order parameter doesn´t vanish any more at the interface (see eq. (1.15)), showing up as a grey line. The phase locking is not perfect anymore in the Bloch regime and the walls can contain vortices. This indicates that the phase is allowed to display smooth variations.

In the nonvariational case both structures are still found for small values of α and ν but while in the variational case both types of walls are static, Bloch walls now move.
Numerically the analytic solutions are affirmed (see figure 1.28).

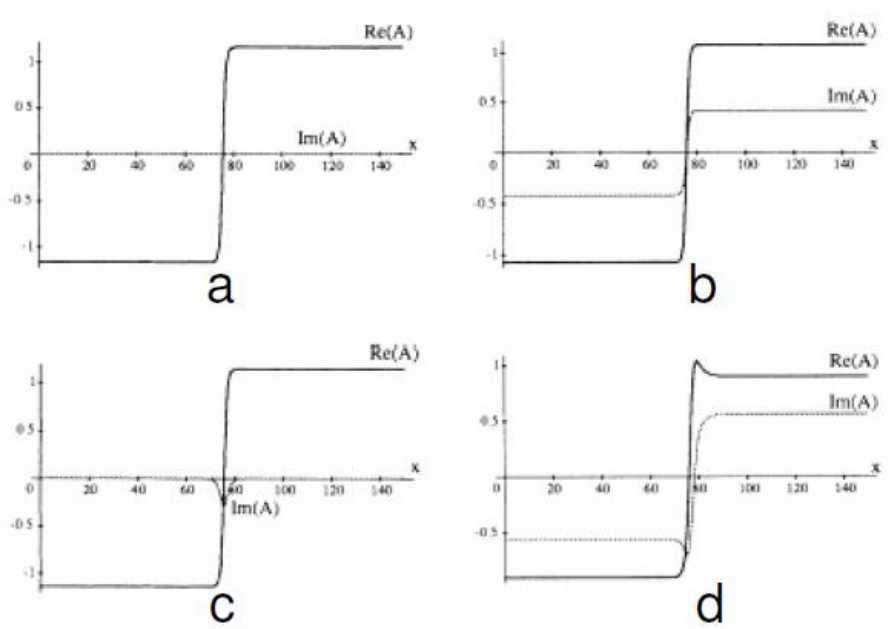

Figure 1.28: Numeric integration of the GLE with Rocking. Variational case (a) and (b), nonvariational case (c) and (d). Left column: Ising walls, right column: Bloch walls. Image taken from [2].

In figure 1.29 the effect of rocking is demonstrated numerically and experimentally for the one-dimensional case.
Studying the one-dimensional case allow understanding the character of the phase defects forming the patterns in spatially extended system avoiding effects of curvature. In two spatial dimensions curvature effects lead to the contraction of phase domains.

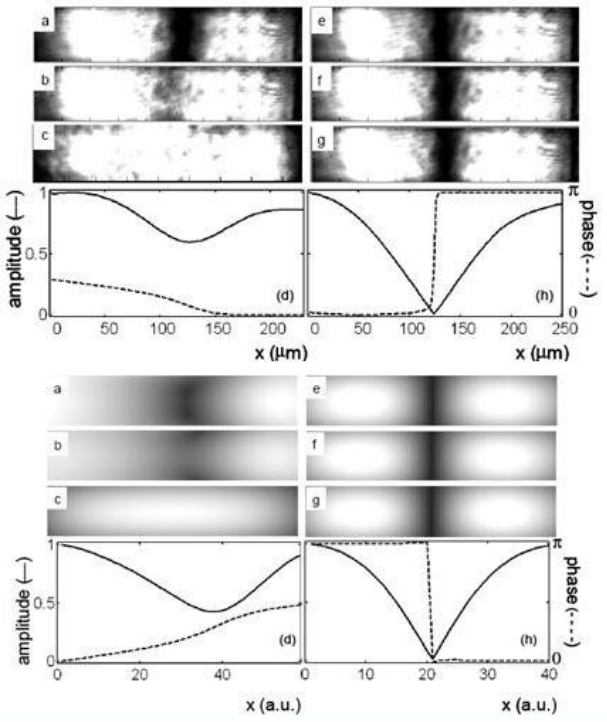

Figure 1.29: Injected domains walls eventually disappear in complex systems (left column) while they are sustained when Rocking is applied (right column). Upper part: experimental results, lower part: numeric simulations. Image taken from [6].

Two-dimensional solutions:

In two dimensions there are no analytic solutions possible any more and the equations have to be integrated numerically. Below some numeric simulations for the nonvariational case and rocking frequency not much larger than one $\omega = 4\pi$ are presented. In the following $\alpha = 10$ ($\alpha >> 1$ is typical for nonlinear optics, where dispersion is strong).

There are different kinds of patterns depending on the detuning parameter ν and the Rocking strength:

$\nu = 0$*:*
The case of zero detuning $\nu = 0$ is shown in figure 1.26.
Without driving ($F = 0$) a chaotic ensemble of vortices separated by shock waves (shock waves are typical in the case of high dispersion) is observed (fig. 1.26 a).
When rocking is not applied the system is described by the CGLE and shows the kind of patterns presented in section 1.7.

For large rocking strengths phase domains separated by Ising-like walls appear (similar to fig.1.27 b).

For weaker rocking Bloch walls appear (similar to fig.1.27 a).

These walls exhibit random evolution. They are highly unstationary due to the curvature effects.

Both in the variational and the nonvariational case Ising and Bloch walls contract until a homogenous state with a single phase is left. A similar dynamic behavior was found for the domains described by the RSHE in section 1.8.

$\alpha\nu > 0$:
For $\alpha\nu > 0$ extended patterns can be excited (compare with fig.1.20). Ising-like and Bloch-like labyrinths are shown in figure 1.30 a and b respectively.

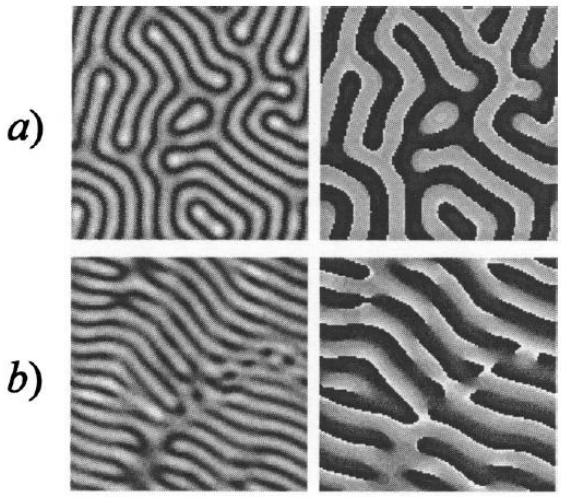

Figure 1.30: Numeric simulations for positive detuning in the nonvariational case show (a) Ising-like and (b) Bloch-like labyrinths. Left column: amplitude, right column: phase. Image taken from [4].

For values of ν between those of contracting domains and those for labyrinths, spatial solitons are found (see figure (1.31)). The stable and stationary solutions for intermediate values of detuning were also found for the RSHE (see figure 1.18).

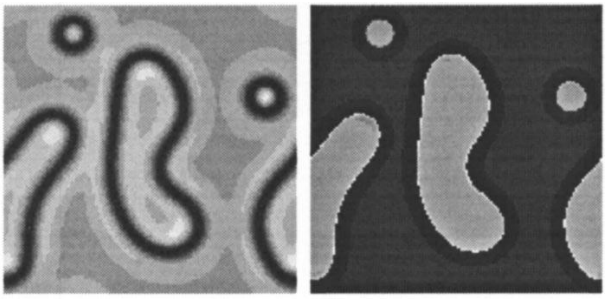

Figure 1.31: Two stable solutions (rings) and two contracting domains for a detuning parameter smaller than in figure 1.30. The domains contract until finally four solitons are left. Image taken from [4].

1.9.3 Spatial Rocking

Spatial Rocking is a monochromatic forcing close to the main resonace of the system where the amplitude of the forcing is spatially modulated.

This is at difference to Temporal Rocking which is based on a forcing with temporary modulated amplitude as presented in the section above. The modulation frequency of the amplitude of the Temporal Rocking beam can be too close to eventual relaxation oscillations in certain optical cavities.
Resonance phenomena can be expected that could affect the phase locking if Temporal Rocking is applied at a frequency close to the relaxation oscillation frequency or it´s harmonics and subharmonics. Locking regimes for different lasers were studied in [7] and it turned out, that in class B lasers the response is strongly modified, because Temporal Rocking is at a frequency close to relaxation oscillations.
This section is based on [1], where this novel technique as alternative to the Temporal Rocking is presented. In this article analytic and numeric results are discussed for the one-dimensional case.

Spatial Rocking is supposed to lead to similar effects as Temporal Rocking, but couldn´t be experimentally realized yet. Actually there´s a group at the Optical Department of the University of Valencia working on that.

The Spatial Rocking technique can be applied to systems that include arrays of coupled oscillators (e.g. Josephson-junction arrays), reaction-diffusion oscillatory systems (certain chemical reactions) and optical systems with large Fresnel number (e.g. lasers or optical parametric oscillators).
In the case of lasers Rocking is one of the few ways to induce phase bistability.
Excitation of stable spatial solitons can be used in optical information storage and processing.

In the following the conversion of an initially complex system into a real-like one via Spatial Rocking is demonstrated. A spatially extended system that shows a spontaneous transition into an oscillatory state via a homogenous Hopf bifurcation is considered.

The mechanism is based on a parametric forcing in a $1:1$ resonance, where the amplitude of the forcing has an alternating sign across the system.
The spatial modulation can be random as long as the dominating spatial scale is much shorter than the scale of the emerging structures.

Without amplitude modulation, the forcing in a $1:1$ resonance imposes a single phase to the system. If the amplitude is modulated like in the Spatial Rocking the injection has two phases that alternate across the system.
If this happens on a short spatial scale, the system can´t "decide" for neither of the two phase values, but sees both.
Assuming, that on average the two phases are equally distributed, the system locks to any of them. Hence it behaves bistable in phase.
The bistable spatially extended system can form a variety of dissipative structures which are controlled by the detuning between the frequency of the forcing ω_f and the system´s natural

frequency of oscillations ω_0.

For small detunings and close above oscillation threshold the dynamics of the system order parameter $A(\vec{r},t)$ can be described by:

$$\frac{dA}{dt} = (1+i\theta)A + \alpha\nabla^2 A - \beta)A\,|A|^2 + F(\vec{r}) \tag{1.16}$$

$\nabla^2 = \delta_x^2 + \delta_y^2$...when z is the direction of propagation
θ... detuning parameter
β....saturation (nonlinear frequency shift) coefficient
α...diffusions (diffraction) coefficient

This is a dimensionless CGLE, similar to eq. (1.10) but now with spatially modulated forcing.
Eq. (1.16) is written in terms of the external forcing frequency. The actual order parameter is proportional to $A = A(\vec{r},t)\cdot e^{-i\omega_f t}$ and the actual forcing is proportional to $F = F(\vec{r})\cdot e^{-i\omega_f t}$.

For the following analytic discussion the limit of short spatial variation of $F(\vec{r})$ is considered:

$\vec{R} = \epsilon^{-1}\vec{r}$, with $\epsilon << 1$.

Furthermore the forcing has to be large, because it is not spatially resonant.
Then a series expansion of $A(\vec{r},t)$ in orders of epsilon can be done.

Under these assumptions the solutions of eq. (1.16) are of the form

$A = A_F + a + O(\epsilon)$.

A_F is the system´s trivial response to the external forcing and related to the external forcing by

$\alpha\nabla^2 A_F = -F$.
a is found from a solvability condition that has to be imposed at order ϵ^0 of the series expansion and reads:

$$\frac{\delta a}{\delta t} = (1+i\theta-2\beta\gamma')a + a\nabla^2 a - \beta|a|^2 a + \beta\gamma a^* \tag{1.17}$$

With $\gamma = -\left\langle A_F^2\right\rangle$ and $\gamma' = \left\langle |A_F|^2\right\rangle$.

Eq. (1.17) is a CGLE with the additional term $\beta\gamma\alpha^*$ that implicates the rupture of phase

invariance. This equation is again of the type of eq. (1.9), that describes parametric driving of a self-oscillating system at a 2:1 resonance.
Thus expected localized structures are dissipative solitons and domain walls and extended patterns are rolls.

When the driving is not periodic but random, the mechanism still is effective, but in this case simulations show that localized structures gather at some preferred locations.

CHAPTER 2

Nonlinear Optical Cavities (NLOCs)

The following sections 2.1-2.2 are based on [2], [17] and [5]. Figures **??** -2.2 are the result conclusions I made myself.

A realization of an optical system showing the kind of structures described so far are Nonlinear Optical Cavities, e.g. lasers or Optical Parametric Oscillators of large Fresnel number.

For the experiments described in this project a photorefractive oscilator (PRO) is used. There are certain advantages in using a PRO instead of a laser with conventional nonlinear medium while the experimental results are valid for both.

The theoretical model has to be slightly adapted and there are some perculiarities going with the photorefractive theory (see 2.3), but this doesn´t affect fundamental results.

2.1 Basic scheme of NLOCs

A nonlinear optical cavity basically consists in a pair of mirrors and a nonlinear medium in between of the mirrors (see figure 2.1).

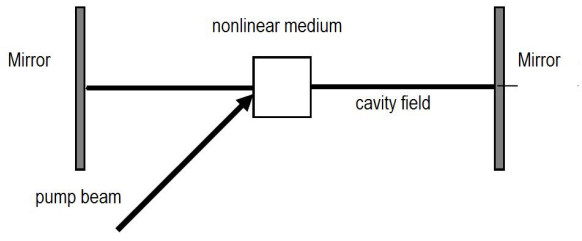

Figure 2.1: Basic scheme of a nonlinear optical cavity on the example of a Fabry-Perot resonator.

Form and position of the mirrors impose the border conditions to the optical system and determine the structure of modes supported by the system.

The pair of mirrors constitutes the cavity and provides the realimentation of the light inside the cavity. Strong realimentation causes the light captured between the mirrors to pass many times through the nonlinear medium.
This leads to the fact that the system doesn´t perform a simple nonlinear transformation of the light passing under certain border conditions only once through the nonlinear medium. The cavity makes the system a dynamic one that evolutes and shows it´s proper distribution not present in the initial conditions. This enables to observe spontaneous symmetry breaks and self-organization phenomena.

2.2 Classification of nonlinear optical cavities

Since the type of radiation emitted by a resonator depends on many factors, it is useful to distinguish classes of optical cavities concerning different properties.

Nonlinear optical cavities can be classified by:

- the geometry of the resonator (linear or ring resonator, shape of the mirrors, low or high Fresnel number etc.)
- the relative values of the constants of relaxation (type A, B or C)
- the kind of interaction of the radiance and the medium inside the cavity (active or passive systems, photorefractive cavities etc.)
- the type of order parameter equation (OPE) describing them

The kind of structures and patterns in the transversal plane of the cavity electric field depend furthermore sensitively on other system parameters like light intensities, cavity detuning, pump beam geometry or the type of injection.

All this gets reflected in the kind order parameter equation describing a cavity in particular.
Since we are interested in the patterns displayed by a cavity a differentiation concerning the type of OPE is the most useful in our case.

The main requirements to a nonlinear optical cavity to emit the patterns described by the order parameter equations presented in the sections above (sections 1.7 - 1.9) are

- to represent a spatially extended system that shows
- essentially nonlinear pattern formation
- and is continously detunable.

In concrete this requires

(1) a sufficiently large Fresnel number of the resonator and

(2) filtering in the far field (Fourier space).

Under these conditions the light in the cavity provides several resonant images in the transversal plane of the cavity field while different points on the plane can be regarded as linearly independent. All types of relation between different points on the transversal plane of the cavity field can then be considered of nonlinear origin which provides the prerequisite of nonlinear pattern formation. Filtering in Fourier space allows studying the patterns depending on the detuning parameter as described by the RSHE and CSHE.

Large Fresnel number cavities :

The Fresnel number is a measure for diffraction and reads

$F = \frac{a^2}{L \cdot \lambda}$

a^2... characteristic size of the aperture
L... distance between the aperture and the screen
λ... incident wavelength

In the case of optical resonators, a^2 is the area of the mirrors of the resonator and L is the length of the resonator.
For a particular wave length, a large Fresnel number is given when the so called *large ratio aspect* is provided. The boarders of the mirror 'are seen' under a very large angle and diffraction due to finite mirror size becomes negligible. In a limit the mirrors seem to be infinitely large (zero cavity length $L = 0$), representing a cavity that imposes no transversal border conditions.

The smallest spatial scale of patterns due to diffraction is related to the Fresnel number by ([3])

$x/x_{aper} = x_{min} = F^{-1/2}$

x... spatial dimension in which the patterns are produced
x_{aper} is the width of the aperture

In large Fresnel number cavities diffraction due to finite mirror size can be considered to be zero and geometrical optics is appropriate to describe the cavity field (paraxial approximation, no crossing of light beams within the resonator).

Experimentally a large Fresnel number cavity can be realized with a *Quasi-Self Imaging* configuration.
Such a configuration is presented in more detail in section 2.5. Patterns due to diffraction now scale with the effective resonator length which is given by the distance between the images of the resonator mirrors. The quasi-self imaging or quasi-auto imaging configuration presents several

advantages concerning practical reasons. Since the mirrors are projected on the site of the crystal via two telescope systems, the real resonator length is not changed, hence there is space enough to introduce several devices into the cavity. This setup furthermore provides the possibility of filtering in the Fourier plane. The far field plane corresponds to the focal plane of the telescope systems making it accessible on the experimental desk.

A **spatially extended system** is optically respresented by a transversally degenerated single longitudinal mode. Transversal degeneracy means that there is a set of resonant modes with the same resonant longitudinal spatial frequency $|k_{long}|$ but different transversal spatial frequency $|k_{trans}|$ as presented schematically in figure 2.4. Due to radial symmetry there is a whole family of modes with different $\vec{k}_{trans}$ for a certain value of $|k_{trans}|$, forming a cone of light as presented in figure 2.2.

Experimentally such a mode structure can be achieved with concentric or confocal resonators when they are exactly tuned to one of their cavity modes. This corresponds to a plane resonator with infinitely large Fresnel number (zero cavity length $L = 0$) or more generally a *quasi-self imaging* configuration.

When spherical resonators are not exactly tuned a ring system occurs in the far field comparable to the Fabry-Perot rings in the case of a plane resonator with finite cavity length. These rings are due to interference between beams of equal frequency and are visible in cavities of finite cavity length L. Constructive interference occurs under those angles, where the phase of a mode reproduces itself in one cavity roundtrip. The higher the Fresnel-number the larger is the width of the rings. In large Fresnel number cavities the central spot of the ring system covers the transversal extension of the system. The cavity field can mathematically be described by one single wave-vector and a slowly varying amplitude, that´s a mono-frequent paraxial beam of large diameter.

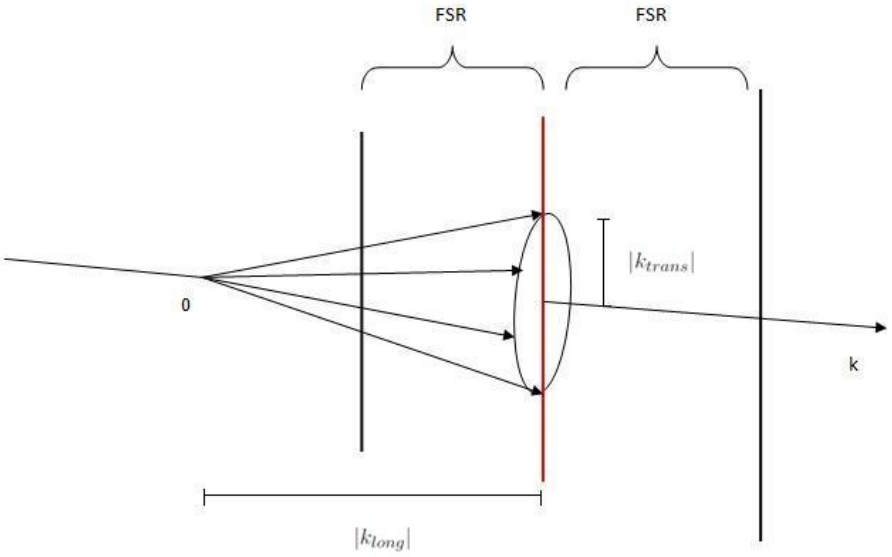

Figure 2.2: Modes with longitudinal component $|k_{long}|$ and transversal component $|k_{trans}|$ lie on a cone.

Total transversal degeneracy of a longitudinal mode is achieved, when the cavity field is not influenced by transversal borders (due to finite mirror size). This is provided in resoantors in self imaging configuration (L=0). Under such conditions to each point on a plane normal to the cavity field corresponds a different mode.
Within a particular mode the phase is related (light propagation by diffraction is a linear process) but the phases of different modes are not. Different modes can be regarded as independent concerning linear processes Thus different points of a screen put in the normal plane of light propagation provide linearly independent information (phase values). If phase patterns occur under such conditions they are due to **nonlinear interactions** between the modes.

Deviations from the ideal conditions (zero diffraction, perfect transverse mode continuum) cause diffraction on system components and interference phenomena. This gets reflected in the spectrum of the modes in the Fourier space.
To realize the single longitudinal and multi-transversal mode case described by the SHE filtering in the Fourier plane (far field) is necessary to select a continuous spectrum of transverse modes and eliminate linear effects. Patterns appearing in the transversal plane under such conditions depend on the tuning parameter only. Occurring diffraction can be considered in equations (1.1) or (1.4) by a nonzero diffraction coefficient a, if the variation of the resonator length is small compared to the length in the case of zero detuning.

In order to study the influence of the tuning parameter on the type of patterns described by the RSHE and CSHE, the system has to be **continuously detunable**.
In particular it is required that within a large range of deviations from exact tuning concerning a certain frequency the cavity stays resonant.
Within a small range the resonator can maintain resonance for the light of a particular frequency when detuned in length by $\Delta L > 0$ through emission out of axis, as presented in figure 2.3.

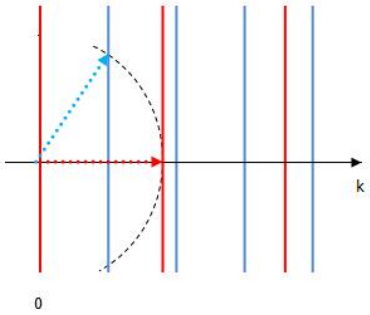

Figure 2.3: When the length L of exact longitudinal resonance for a particular resonator mode (red flecher and red vertical lines) is changed by $\Delta L > 0$, the mode spectrum changes from the red to the blue one. Resonance can be maintained through emission out of axis (blue flecher).

In cavities in quasi-self imaging configuration, the longitudinal resonator modes are highly degenerated in transversal frequency (see fig. 2.4) due to the large aspect ratio. The resonator stays resonant for any value of detuning until losses due to diffraction become too large. The effect of inclination ot the modes to maintain resonance described by figure 2.3 overlap as the transverse mode spectrum becomes sufficiently narrow.

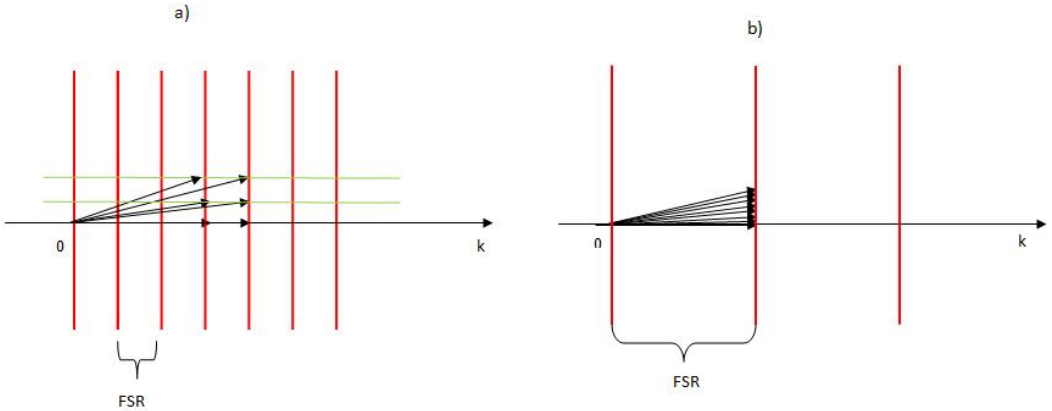

Figure 2.4: Resonant modes for resonators of different lenght and mirror size: Vertical lines represent the longitudinal modes of the resonator. Horizontal lines represent the transversal resoantor modes (only indicated in a)). Wave vectors with zero transversal component are longitudinal modes. Flechers with equal longitudinal wave vector components represent the corresponding transversal modes. From a) to b) the length of the resonator was changed by $\Delta L < 0$ and the area of the mirrors was increased. As a consequence the FSR becomes larger and transversal modes lie closer.

A cavity of special interest for this project is the *linear Fabry-Perot resonator in quasi-self imaging configuration* (figure 2.29).
The reason for using a Fabry-Perot resonator is that the experiment is particularly simple in a cavity with planar mirrors in linear configuration.

In the case of the planar cavity one can relate the pattern forming properties of the system to the ones of other pattern forming systems and describe them universally by order parameter equations like the Ginzburg-Landau equation, the Swift-Hohenberg equation, etc.. The simple geometry allows furthermore a simple theoretical treatment in the image procession. Linear - and therefore comparably simple - image processing is possible.

On contrary to a cavity with spherical mirrors the planar cavity can be adjusted to the exact resonace length for any frequency.

In near-self-imaging configuration the transverse modes are almost totally degenerated and the cavity is continuously detunable while resonance is maintained. This allows studying the influence of the detuning on the kind of patterns.

Another advantage of the planar cavity is that in comparison with a focalizing cavity a planar cavity makes use of a larger region of the laser medium.

2.3 The photorefractive oscillator (PRO)

The setup of a photorefractive resonator (PRO) is equivalent to a laser cavity, but instead of the conventional nonlinear medium, there is a photorefractive crystal used as active medium.
The physical processes to generate the oscillation field are different, but the PRO model of purely diffusive photorefractive materials (such as $BaTiO_3$) is largely equivalent to the one of large aspect ratio class A lasers from the nonlinear dynamics point of view.
Hence the cavity field of a PRO is described by order-parameter equations of the same type as presented in the sections above [8].

The advantage of a photorefractive crystal as nonlinear medium is twofold.
The temporal evolution of the patterns occurs on a time scale given by the response time of the photorefractive material. Since the photorefractive effect is rather slow (in PROs the dynamic processes happen in the range of seconds, while in lasers they happen in μs) it is possible to record the dynamics with charge coupled devices, which provides a simple and cheap manner of recording.
On the other hand a PRO is very efficient. Conventional nonlinear media require intensities in the range of MW/cm^2, while the most efficient photorefractive materials like $BaTiO_3$ or $LiNbO_3$ require intensities in the range of $1W/cm^2$ ([19]).

The information for the theoretical background of the photorefractive effect in sections 2.3.1-2.4 is taken from [18] and [19].

2.3.1 Introduction to photorefractive nonlinear optics

Photorefractive nonlinear optics differ from nonlinear optics of conventional nonlinear media in several aspects.
One example is the non-reciprocal energy transfer between beams of light within the nonlinear medium as it happens between the pump beam and the light in an optic resonator.
In photorefractive optics this process has to be described by the different microscopic model as it is used for conventional nonlinear media (Kerr media).
In lasers the energy transfer from the pump beam to the lasing beam is due to absorptions in the active medium (transitions between atomic states of the active medium), while the energy transfer in photorefractive oscillators (PROs) is due to the Photorefractive Effect.
This effect is explained by Bragg reflections of light of spatially non-uniform intensity on a self induced index pattern in the photorefractive material.
The change in the index of refraction of the photorefractive medium plays a key role in photorefractive cavities. The processes that lead to this change in the index of refraction mark another difference to conventional nonlinear media. They cannot be described by a nonlinear susceptibility $X^{(n)}$ for any value of n.

Another difference between lasers and PROs is that in lasers both the pump frequency and the signal frequency are determined by the active medium. The frequency of the pump beam and the one of the signal beam usually differ a lot from each other.
In a photorefractive cavity the emitted frequency is the same or lies close to the frequency of the pump beam. There is coherence between all involved beams in photorefractive processes.

Finally there should be mentioned, that on contrary to lasers, a PRO can maintain resonance in any sense of detuning. While lasers have a minimum resonance frequency corresponding to $L = \lambda/2$ and resonance via emission out of axis (see 2.2) for frequencies below this smallest resonator mode is not possible, a PRO can stay resonant due to the so called photorefractive phase shift (see theory below).

2.3.2 The Photorefractive Effect

Photorefractive Effect is called the nonlinear macroscopic phenomenon that can happen in electrooptic crystals where the linear index of refraction experiences local changes $\Delta n(\vec{r})$ due to the illumination with light of a spatially varying intensity distribution.

The change in the index of refraction is induced via the linear electrooptic effect (Pockels effect) and results from the optically induced redistribution of electrons and holes. The light suffers diffraction on a self induced index pattern and energy coupling between coherent beams happens automatically as a generic process.

The photorefractive effect was first observed in 1966, when laser physics came up and coherent light of high intensity could be generated, so that the nonlinear processes in photorefractive materials could be observed. Historically the distortion of the wave front of the laser beam that passed an electrooptic material was called optical damage. The photorefractive effect was then found in many electrooptic materials, including el $BaTiO_3$, which was used in our experiment.
Most of the observed photorefractive phenomena can be described by a microscopic model named Band Transport Model which will be presented in the section 2.3.3.
Once obtained the expression for the induced changes $\Delta n(\vec{r})$ of the refraction index, solutions for the optical field inside the photorefractive material can be obtained using Maxwell equations.

2.3.3 The Band Transport Model for Photorefractive Materials

The medium is considered to have a bandgap and impurities with energy states somewhere in the middle of the bandgap. There are impurities that can be photo-ionized by incoming light working therefore as donors, generating electrons in the conduction band. The electrons can be captured by acceptor impurities.
Due to a charge gradient, the electrons that are excited into the conduction band in the illuminated regions of the material drift to the dark regions, where no electrons are excited. If they recombine in a dark region of the material, they will stay there, because there´s no light to re-excite them.
If the incident light is spatially modulated, the donor impurities in the illuminated regions get ionized, that´s positively charged and in the dark regions the negative charge is accumulated.
The charge separation causes a space charged field which will change the index of refraction through the linear electrooptic effect (Pockels-effect).
Figure 2.5 shows a scheme of the band transport model for the photorefractive effect. Donor levels and acceptor levels are supposed to have the same energy.

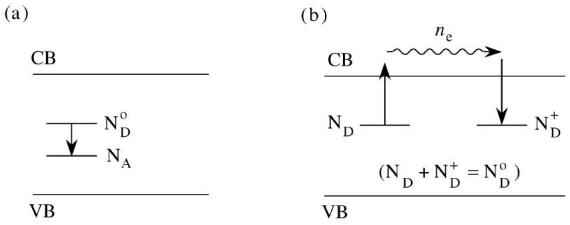

Figure 2.5: Schematic representation of the band transport model for photorefractive materials. The donor and acceptor levels are taken to have the same energy. Image taken from [18].

Periodic Illumination :

A simple and useful way to produce a modulation in the index of refraction by the photorefractive effect is realized by using the periodic fringe pattern of bright and dark stripes generated by the interference of two plane waves of same frequency that form a certain angle with each other.
In fact, this kind of intensity pattern is very representative as it is the one responsible for the effects in the photorefractive cavity used in the experiments described in this master´s project. Here a qualitative description of surveying character is given. A more detailed description of wave mixing processes in photorefractive materials will be done in section 2.4.

The light induced change in the index of refraction is automatically modulated according to variations of the light intensity present in the material. The charge density distribution, the space charged field and index variation in the case of illumination with two plane waves of equal frequency is shown in figure 2.6.

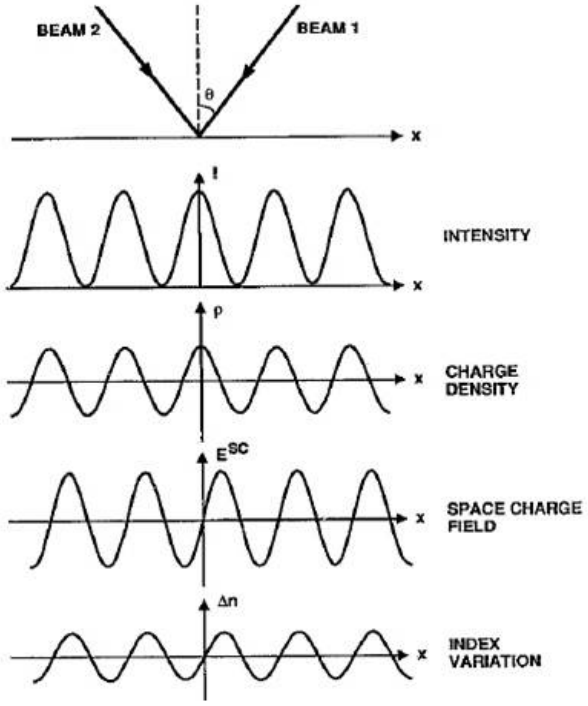

Figure 2.6: Spatial distribution of the light intensity and the induced charge density, space charged field and index variation. In the presented example it is assumed that diffusion is the dominant process. In this case there is a phase shift of $\pi/2$ between the index distribution and the electric field distribution. Image taken from [19].

2.3.4 Photorefractive Equations

Mathematically the band transport model can be expressed by the photorefractive equations of Kukhtarev et al. as they are presented in [18]. These equations provide an adequate description of most photorefractive phenomena.
It is assumed that only one type of charge carrier (in this case electrons with density n_e) dominates the described processes.
The crystal is supposed to contain N_A acceptors and N_D^0 donors per unit volume, with $N_A << N_D^0$ as presented in figure 2.5 (a).
Electrons can be excited thermally or optically from the donor levels into the conduction band (figure 2.5, b).
Variations in level populations $\frac{\delta N_D^+}{\delta t}$ and $\frac{\delta n_e}{\delta t}$ are described by the following rate equations ([18]).

Charge distribution $\rho(\vec{r})$ for a given intensity distribution $I(\vec{r})$:

$$\frac{\delta N_D^+}{\delta t} = (s \cdot I + \beta)(N_D^0 - N_D^+) - \gamma n_e N_D^+ \tag{2.1}$$

$$\frac{\delta n_e}{\delta t} = \frac{\delta N_D^+}{\delta t} + \frac{1}{e}(\nabla \cdot \vec{j}) \tag{2.2}$$

$\frac{\delta N_D^+}{\delta t}$ depends on material constants, the thermal ionization β, the density of donors N_D^0 and the density of ionized donors N_D^+. The change in electron concentration $\frac{\delta n_e}{\delta t}$ is proportional to $\frac{\delta N_D^+}{\delta t}$ and the gradient of a current density $\vec{j}$.
$\frac{\delta n_e}{\delta t}$ can increase locally either due to the ionization of donor atoms $\frac{\delta N_D^+}{\delta t} > 0$ or due to local accumulation of electrons in a region.
The current that leads to such local accumulations of electrons is in the case of materials where diffusion is the dominant process (such as $BaTiO_3$) given by

$$\vec{j} = n_e e \mu \vec{E} + eD\nabla n_e. \tag{2.3}$$

μ ..... electron mobility
$D = \frac{k_B T \mu}{e}$ .... diffusion constant
$\vec{E}$ .....static (or low-frequency) electric field

The electric field $\vec{E}$ accounts for any externally applied voltage or charge separation within the crystal. In the case of our experiments, where no external voltage was applied, the electric field is given by $\vec{E} = \vec{E}_{sc}$. $\vec{E}_{sc}$ is the space charge field due to the charge separation.

Once obtained the charge distribution by equations (2.1) - (2.3), the space charge field $\vec{E}_{sc}$ can be calculated from Gauss´ law:

$$\epsilon_{st} \nabla \vec{E}_{sc} = -e \cdot (n_e + N_A - N_D^+) = -e \cdot \rho(\vec{r}). \tag{2.4}$$

ϵ_{st}..... static dielectric constant
n_e..... electron density
N_A..... density of accaptor atoms
N_D^+.... density of ionized donor atoms

The Space Charge Field and spatial phase shift:

The spatial derivative that appears in this equation leads to a spatial phase shift between the charge density distribution $\rho(\vec{r})$ and the space charge field $\vec{E}_{sc}$. In general this phase shift depends on whether the interfering beams have exactly the same frequency and on the presence of an additionally applied external electric field.

In the example considered here (figure 2.6), that´s materials where diffusion is the dominant process (as for $BaTiO_3$) and illumination with the periodic fringe pattern produced by two monochromatic plane waves, this phase shift is $\pi/2$.

In steady state the diffusion currents are counterbalanced by the drift currents and the space charge reads

$$\rho = \rho_0 \cdot cos(\vec{K}\vec{r}). \tag{2.5}$$

ρ_0..... charge density without illumination
$\vec{K}$..... grating wave vector of the fringe pattern produced by two beams as given by eq. 2.11

Spatial integration of Gauss´ law (eq. 2.4) gives the space charge field:

$$\vec{E}_{sc} = \rho_0 \cdot \frac{\vec{K}}{\vec{K}\epsilon\vec{K}} \cdot sin(\vec{K}\vec{r}) \tag{2.6}$$

The phase shift between the charge density distribution and the space charge field due to the Gauss law allows a nonreciprocal steady-state transfer of energy between the beams that form the intensity pattern. This can be seen from the coupled equations (2.28) and (2.29), when introducing the expression of the modified dielectric constant (2.7) into the wave equation (2.8).

Since the photorefractive effect is macroscopic, a large number of charge carriers is needed, typically in the order of $[10^{15}cm^{-3}]$. For typical parameters for photrefractive crystals: $N_A = 10^{16}cm^{-3}$, $\langle\epsilon\rangle = 10 \cdot \epsilon_0$ and $T = 300K$, the maximum space charge field E_sc is $E_{scmax} = 0.34 * 10^6(V/m) \cdot I/I_0$.

Modification of the optical material properties due to the Pockels Effect:

The modification of the dielectric constant is due to the linear electrooptic effect (Pockels effect). The Pockels effect is the fundamental component oft the intensity induced changes in the dielectric constant. In general it has to be described by a third-rang tensor, since the effect depends on the direction of the space charge field and the polarization state of the light.
In the principal coordinates of the dielectric tensor ϵ the Pockels effect reads

$$\Delta\epsilon_{ij} = -\epsilon_0 n_i^2 n_j^2 r_{ijk} \cdot \vec{E}_k \tag{2.7}$$

ϵ_0..... vacuum dielectric constant
n_i, n_j... principal indices of refraction
r_{ijk}..... electrooptic coefficients (give the rate at which the coefficients $1/n_i^2$, $1/n_j^2$ change with increasing electric field strength)
$\vec{E}$... static (or low frequency) electric field

Finally the optical field in the photorefractive material is obtained from the homogenous wave equation

$$\nabla^2 \vec{E}_{opt} + \frac{1}{c^2}\frac{\delta^2}{\delta t^2}(\epsilon_{st} + \Delta\epsilon_{ij})\vec{E}_{opt} = 0. \tag{2.8}$$

c.....velocity of light
ϵ_{st}...static dielectric constant
$\Delta\epsilon_{ij}$ from equation

2.4 Wave Mixing in Photorefractive Materials

The photorefractive equations 2.1-2.4 usually can´t be solved exactly since they are nonlinear functions of unknown variables. Nonetheless there are analytic solutions for a variety of special cases.
In this section analytic expressions for Two- and Four-Wave-Mixing (TWM and FWM respectively) in photorefractive materials will be presented. TWM and FWM are the fundamental processes happening in a photorefractive resonator.

Beam coupling, beam fanning and the photorefractive phase shift play a central role in photorefractive cavities. Energy from the pump beam is transferred to the cavity field as a consequence of beam coupling in the photorefractive medium. Beam fanning plays a key role in the initiation processes of the cavity field and the photorefractive phase shift admits conditions of resonance in a wide range of both positive and negative detuning.

Two-beam coupling and energy transfer:

Under certain circumstances, two beams can interact in such a manner that energy is transferred from one beam to the other which leads to the weakening of one beam and the amplification of the other beam. The efficiency and the direction of the energy flow depend on several factors.

The transfer of energy can happen between two incident beams of coherent light in nonlinear material or periodic structures, whenever there´s a phase shift (temporal or spatial) between the incident light and the material response and phase matching conditions are fulfilled. Under conditions of perfect phase matching the efficiency of the energy transfer process is maximum.
Weather the transfer of energy is symmetrical or non-reciprocal depends on the phase shift between the two beams.
The mathematical description of beam coupling is done by introducing the total index of refraction into the wave equation, which leads to coupled equations in the case of periodic or nonlinear materials under certain conditions.

Bragg theory for beam coupling in periodic structures:

If light propagates trough inhomogenous media diffraction occurs. If the inhomogeneities are periodic the diffraction occurs in a directed sense, where there is a reflected and a diffracted part of the light. Similar as for x-rays passing condensed matter there is a Bragg law describing the angle of maximum reflection. The reflection of light by a periodic index modulation is described by coupled equations (the incident beams gets diffracted in the direction of the reflected beam and energy is transferred) as it can be seen when the periodic index of diffraction is introduced into Maxwell equations.
There´s is a transfer of energy between the incident and diffracted beam, whereas the efficiency of the process depends on the amplitude of the index variation and on a phase matching factor. Perfect phase matching is achieved when Δ_k becomes zero that´s when diffraction occurs under perfectly fulfilled Bragg condition.

When the index grating is due to the periodic fringe pattern of two coherent plane waves, the Bragg reflections on the self-induced index pattern are perfectly phase matched. The refractive index experienced by either wave is modified by the intensity of the other wave. Each beam gets diffracted in direction of the other beam. The total energy beam one is transferred to beam 2 and vice versa. Bragg condition is perfectly fulfilled for two beams that diffract of a grating formed by themselves. This is known as *autodiffraction* (figure 2.7).
Without a phase shift between the intensity- and the index-patterns, the energies of beam one and two are transferred symmetrically. For energy being transferred in a non-reciprocal way, there is a nonzero phase shift between the light- and the index-pattern necessary.

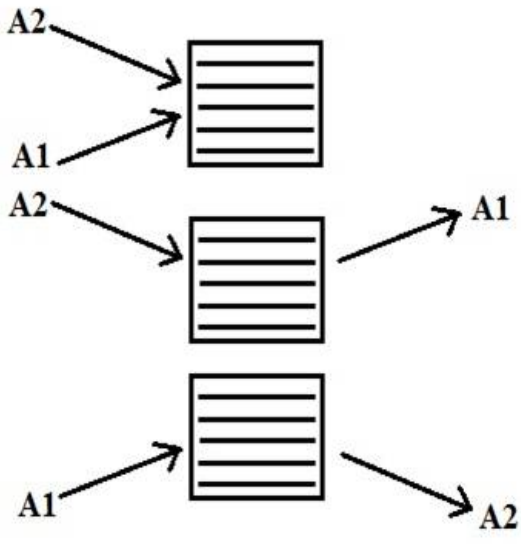

Figure 2.7: Autodiffraction of beams A1 and A2 on an index grating produced by themselves. Beam A1 gets diffracted in the direction of beam A2 and vice versa. Image taken from [19].

In conventional nonlinear media (Kerr media) coupling between beams is due to a higher order susceptibility. The refraction index is proportional to the intensity of the light inside the medium - i.e. the total index of refraction is a nonlinear function of the incident electric field.

$$N = n_0 + n_2 \cdot I \tag{2.9}$$

n_0.....linear refraction index
n_2.....Kerr coefficient.
I..... Intensity

The interference pattern formed by the two coherent beams causes an index pattern via eq.(2.9). Inserting this expression into Maxwell equations leads to an inhomogeneous wave-equation which are approximately solved by two plane waves with coupled amplitudes.
Since the index pattern is produced by the beams themselves phase matching is perfectly fulfilled. Nonreciprocal energy transfer requires a non-zero phase between the intensity pattern of the light inside the medium and the index pattern due to the light pattern.

In Kerr media such a phase shift between the intensity- and the index-patterns can´t be spatial, since the dependence of the local index of refraction on the intensity is described by eq.(2.9). Thus the required phase shift necessarily has to be temporal which implicates a non-instantaneous material´s response to a moving index grating. Moving gratings are formed between beams of different frequency (non-degenerate beam coupling) an the non-instantaneous response is given in materials where the built up of the change in index due to intensity is described by a Debye law.
Hence in homogenous Kerr media there is no energy transfer possible between beams of light with the exactly the same frequency (degenerate beam coupling). Degenerate beam coupling can only happen between an incident beam of light and its diffracted part in the case of propagation through a periodic Kerr medium, when the periodicity is not self-induced by the incident light, but the structure of the material itself without illumination.

On contrary in photorefractive material beam coupling happens automatically for both non-degenerate and degenerate wave mixing. This is due to a generic spatial phase shift between the intensity- and the index-pattern. As the phase shift is spatial, there is no temporal phase shift required and energy transfer is possible even in the case of degenerate wave mixing.
In photorefractive materials modifications of the index of refraction are induced by the gradient of an intensity distribution but are independent of the absolute value of the intensity. Non homogenous illumination is a prerequisite to modify the linear index of refraction n_0, since modifications are due to the Pockels effect:

$$\Delta n(\vec{r}) \propto \nabla n_e(\vec{r}) \propto \nabla I(\vec{r}) \tag{2.10}$$

The generation rate of free charge carriers is proportional to the local value of the optical intensity. Introducing the expression for the index of refraction into Maxwell equations leads to a homogenous wave-equation.

The coupling constant depends on the direction of the induced space charge field and the polarization states of the beams before and after diffraction on the self induced index pattern as discussed in the following section.

2.4.1 Two-Wave Mixing (TWM) in photorefractive materials

The illumination is given by the periodic fringe patterns formed by two plane waves of equal or slightly different frequencies (degenerate and non-degenerate TWM respectively) that intersect inside the photorefractive material:

$$\vec{E} = \vec{E}_a \cdot e^{i(\omega_a \cdot t - \vec{k}_a \cdot \vec{r})} + \vec{E}_b \cdot e^{i(\omega_b - \vec{k}_b \cdot \vec{r})} \tag{2.11}$$

Degenerate TWM, $\omega_a = \omega_b$:

$$I(\vec{r}) = I_0 + Re\left\{I_1 e^{-i\vec{K}\vec{r}}\right\} \propto I_1 \cdot cos(\vec{K}\vec{r}) \tag{2.12}$$

$$I_0 = |\vec{E}_a|^2 + |\vec{E}_b|^2 \tag{2.13}$$

$$I_1 = 2\vec{E}_b\vec{E}_a^* \tag{2.14}$$

$$\vec{K} = \vec{k_b} - \vec{k_a} \tag{2.15}$$

$$|\vec{K}| = \frac{2\pi}{\Lambda} \tag{2.16}$$

$\vec{K}$.....grating wave vector
Λ.....period of the interference pattern

In the case of the two plane waves of equal frequencies, there´s a stationary fringe pattern formed.

Inserting this expression of the intensity into the photorefractive equations (2.1)-(2.3) defines the space charge field.
In the following it is assumed that diffusion is the dominant process in the material (as it happens for $BaTiO_3$) and the photovoltaic effect is negligible. Furthermore the case with no applied external fields is considered and in order to find analytic expressions small modulations $|I_1| << I_0$ are assumed.

In the case of maximum fringe visibility, i.e. $\vec{E_a} = \vec{E_b}$, the amplitude of the space charge field in steady state reads

$$E_1 = \frac{i \cdot K \frac{k_B T}{q}}{1 + \frac{K^2}{k_D^2}} \cdot \frac{I_1}{I_0} \propto e^{i\phi} \cdot \frac{I_1}{I_0} \tag{2.17}$$

$k_D^2 = \frac{e^2}{\langle\epsilon\rangle k_B T}\frac{N_A}{N_D}(N_D - N_A)$ is a function of the donor- and acceptor-densities N_D and N_A respectively.

$\langle\epsilon\rangle = \frac{\vec{K}\cdot\epsilon\vec{K}}{K^2}$ is the effective dielectric constant of the material.

In the example of the two monochromatic plane waves and pure diffusion the phase ϕ of the space charge field with respect to the intensity pattern is $\pi/2$ radians as presented in figure 2.6.

One sees that the amplitude of the space charge field is zero if the interference term I_1 vanishes. The amplitude becomes maximum when the fringe visibility does, which happens for $\vec{E_a} = \vec{E_b}$.

The size of $E1$ furthermore depends on the magnitude and orientation of the grating wave-vector.

$$\langle\epsilon\rangle = \epsilon_{||} cos^2\alpha + \epsilon_{\perp} sin^2\alpha \tag{2.18}$$

$$K = 2k \cdot sin\theta \tag{2.19}$$

Where $k = |\vec{k_a}| = |\vec{k_b}|$ is the magnitude of the wave vectors of beams $\vec{E_a}$ and $\vec{E_b}$ and the angles are defined as shown in figure 2.8.

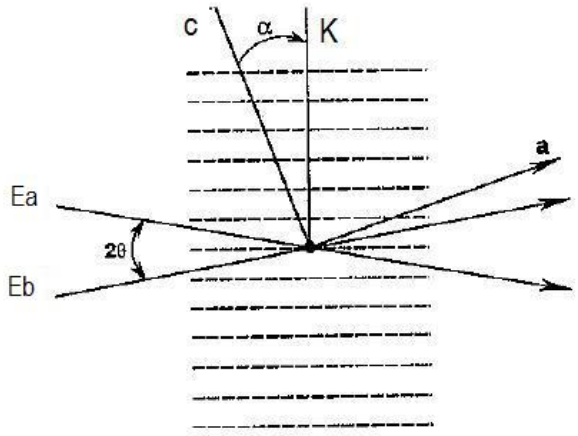

Figure 2.8: Volume grating induced by beams E_a and E_b. The grating wave vector $\vec{K}$ lies in the plane of incidence defined by $\vec{a}$ and the optical axis c. $\vec{K}$ forms an angle α with c. Image taken from [19].

The space charge field is polarized in the direction of the grating vector $\vec{e}_{\vec{K}}$ and spatially modulated with the period Λ.

$$\vec{E}_{sc} = Re\left\{E_1 \cdot \vec{e}_{\vec{K}} \cdot e^{-i\vec{K}\vec{r}}\right\} \tag{2.20}$$

$\vec{K}$.... grating wave vector

Optical modifications due to the Pockels effect:

In the scalar approximation (that´s for ordinary or extra-ordinary waves and assuming that there is no change of polarization due to the scattering process) one can express the modifications of the optical properties due to the space charge field in terms of the index of refraction instead of using the dielectric constant as it was done in eq. (2.7):

$$\Delta n = -\frac{1}{2} n^3 \left\langle \vec{p} | \Delta(\frac{1}{n^2}) | \vec{p} \right\rangle \tag{2.21}$$

With

$$\Delta(\frac{1}{n^2})_{ij} = r_{ijk} \cdot \vec{E}_k^{sc} = r_{ij} \cdot E_1 \cdot sin(\vec{K} \cdot \vec{r}) \tag{2.22}$$

$\vec{E}_k^{sc}$...space charge field as given by eq.(2.20)
$E1$... the amplitude of the space charge field, eq.(2.17), in the scalar approximation
r_{ijk}... the third-rang tensor of electrooptic coefficients
r_{ijk} reduces to the matrix r_{ij} when applied to a particular space charge field.

The direction of $\vec{E}^{sc}$ is parallel to the grating wave vector $\vec{K}$, thus the grating determines which elements of the third rang tensor r_{ijk} are effective in the scattering process.

Equation (2.21) is the effective index grating for the polarization state $\vec{p}$, when no change in polarization occurs due to the diffraction process. n is the index of refraction associated with the polarization state $\vec{p}$. $\vec{p}$ determines which element of the matrix r_{ij}, which is associated with a particular space charge field, is effective in the scattering process of the light.
$BaTiO_3$ has one dominant electrooptic coefficient for space charge fields in y direction and polarization in yz- or equivalently zy-direction. The electrooptic coefficients of some electrooptic materials are shown on table 2.10.

Figure 2.9 shows the electrooptic coefficients for $BaTiO_3$.

$$r_{ij} = \begin{bmatrix} 0 & 0 & r_{13} \\ 0 & 0 & r_{13} \\ 0 & 0 & r_{33} \\ 0 & r_{42} & 0 \\ r_{42} & 0 & 0 \\ 0 & 0 & 0 \end{bmatrix}$$

Figure 2.9: Electrooptic coefficients of crystals of the class 4mm. Here contracted notation is used: $r_{42} \equiv r_{232} = r_{322}$, $r_{13} \equiv r_{113}$, $r_{33} \equiv r_{333}$. Image taken from [18].

Material	Point Group	Electrooptic Coefficients (10^{-12} m/V)	Refractive Index
Potassium dihydrogen phosphate, KH_2PO_4 (KDP)	$\bar{4}2m$	$r_{41} = 8.77$ $r_{63} = 10.5$	$n_0 = 1.514$ $n_e = 1.472$ (at 0.5461 μm)
Potassium dideuterium phosphate, KD_2PO_4 (KD*P)	$\bar{4}2m$	$r_{41} = 8.8$ $r_{63} = 26.4$	$n_0 = 1.508$ $n_e = 1.468$ (at 0.5461 μm)
Lithium niobate, $LiNbO_3$	$3m$	$r_{13} = 9.6$ $r_{22} = 6.8$ $r_{33} = 30.9$ $r_{42} = 32.6$	$n_0 = 2.3410$ $n_e = 2.2457$ (at 0.5 μm)
Lithium tantalate, $LiTaO_3$	$3m$	$r_{13} = 8.4$ $r_{22} = -0.2$ $r_{33} = 30.5$ $r_{51} = 20$	$n_0 = 2.176$ $n_e = 2.180$ (at 0.633 nm)
Barium titanate, $BaTiO_3$ [b]	$4mm$	$r_{13} = 19.5$ $r_{33} = 97$ $r_{42} = 1640$	$n_0 = 2.488$ $n_e = 2.424$ (at 514 nm)
Strontium barium niobate, $Sr_{0.6}Ba_{0.4}NbO_6$ (SBN:60)	$4mm$	$r_{13} = 55$ $r_{33} = 224$ $r_{42} = 80$	$n_0 = 2.367$ $n_e = 2.337$ (at 514 nm)
Zinc telluride, ZnTe	$\bar{4}3m$	$r_{41} = 4.0$	$n_0 = 2.99$ (at 0.633 μm)

Figure 2.10: Optical coefficients of some electrooptic materials. Here contracted notation is used (see figure 2.9 for $BaTio_3$). Image taken from [18].

Using equations (2.22) and (2.21) the change in index of refraction reads

$$\Delta n = -\frac{1}{2} n1 \cdot E_1 \cdot sin(\vec{K} \cdot \vec{r}) \tag{2.23}$$

In the considered case $n1$ is a real number. It includes the linear refraction index n (without illumination) and the electrooptic coefficient r_{ijk} for the concerned polarization state $\vec{p}$ and space charge field $\vec{E}^{sc}$. The sign of $n1$ depends on the orientation of the grating wave vector $\vec{K}$ with respect to the optical axis c of the crystal (figure 2.8).

Comparison of eq.(2.23) with eq.(2.12) shows the phase shift $\pi/2$.

The total index of refraction reads

$$n_{total} = n + \Delta n = n + \frac{n1}{2} \cdot e^{i\phi} \left[\frac{A_1^* A_2}{I_0} \cdot e^{-i\vec{K}\vec{r}} + \frac{A_1 A_2^*}{I_0} \cdot e^{i\vec{K}\vec{r}} \right] \tag{2.24}$$

where $E1$ is taken in the scalar approximation.

Introduction of eq.(2.24)into Maxwell equations leads to the homogenous wave equation

$$\nabla^2 E_{op} + \frac{\omega^2}{c^2} n_{total}^2 E_{op} = 0 \tag{2.25}$$

Hence an ansatz in the form of the incident light is chosen

$$E_{op} = A1 \cdot e^{i(\omega t - \vec{k_1}\vec{r})} + A2 \cdot e^{i(\omega t - \vec{k_2}\vec{r})} \tag{2.26}$$

$$I = |A_1|^2 + |A_2|^2 + A_1^* A_2 \cdot e^{-i\vec{K}\vec{r}} + A_1 A_2^* \cdot e^{i\vec{K}\vec{r}} \tag{2.27}$$

where $A1 = A1(z)$ and $A2 = A2(z)$ are time independent and for reasons of simplicity are taken as functions of one spatial coordinate only. For this sake an infinite beam intersection is assumed such, that the volume grating formed by E_{op} is infinite in y-direction, when propagation in the xz-plane is considered.
The last to summands of eq.(2.27) are the grating terms.

Figure 2.11 shows the volume grating introduced by E_{op} in the case of symmetric incidence. If the angle between the beams inside the material is smaller than $\pi/2$ a transmission grating is formed. If the angle exceeds $\pi/2$ a reflection grating is formed.

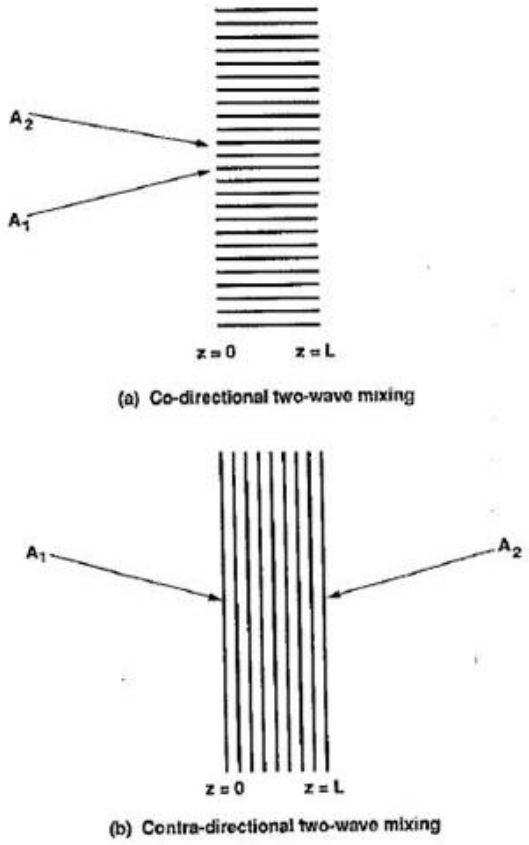

Figure 2.11: Volume grating introduced by beams A1 and A2 into a photorefractive material. a) In the case of a transmission grating co-directional Two-Wave-Mixing happens. b) In the case of a reflection grating contra-directional Two-Wave-Mixing happens. Image taken from [19].

In steady state and using the slowly varying amplitude approximation (assuming a single longitudinal mode and a uniform transversal intensity distribution)

$|\frac{d^2}{dz^2}A_j| << |k_{jz} \cdot \frac{d}{dz}A_j|$, with $j = 1, 2$

the coupled equations for the amplitudes of the optical field inside the photorefractive material read

$$\frac{d}{dz}A_1 = \frac{-i}{2k_{1z}}\frac{\omega^2 n_0 n_1}{c^2 I_0}e^{-i\phi}A_2^* A_1 A_2 \tag{2.28}$$

$$\frac{d}{dz}A_2 = \frac{-i}{2k_{2z}}\frac{\omega^2 n_0 n_1}{c^2 I_0}e^{i\phi}A_1^* A_2 A_1 \tag{2.29}$$

k_{2z}, k_{2z}.....z-components of the wave vectors

Here one sees the influence of the size of Δn on the coupling between the amplitudes and the influence of the phase ϕ, which is the phase shift between the intensity and the index-patterns.

For vanishing ϕ there is no net-energy flow from one beam to the other.

Dependent on whether the formed grating is a transmission grating or a reflection grating (figure 2.11) there is co-/ or contra-directional 2WM happening:

Co-Directional TWM: $k_{1z} \cdot k_{2z} > 0$

$A_1 = \sqrt{I_1}e^{-i\psi_1}$ and $A_2 = \sqrt{I_2}e^{-i\psi_2}$

$$\frac{d}{dz}I_1 = -\gamma\frac{I_1 I_2}{I_1 + I_2} - \alpha I_1 \tag{2.30}$$

$$\frac{d}{dz}I_2 = \gamma\frac{I_1 I_2}{I_1 + I_2} - \alpha I_2 \tag{2.31}$$

$$\frac{d}{dz}\psi_1 = \beta\frac{I_2}{I_1 + I_2} \tag{2.32}$$

$$\frac{d}{dz}\psi_2 = \beta\frac{I_1}{I_1 + I_2} \tag{2.33}$$

$$\Gamma = \gamma + i2\beta \tag{2.34}$$

$$\gamma = 2\frac{\pi n1}{\lambda cos\theta}sin\phi \tag{2.35}$$

$$\beta = \frac{\pi n1}{\lambda cos\theta}cos\phi \tag{2.36}$$

2θ... angle between the beams inside the material
α... absorption coefficient
$n1$...as described by eq.(2.23)
ϕ...phase shift between the intensity pattern and the index grating

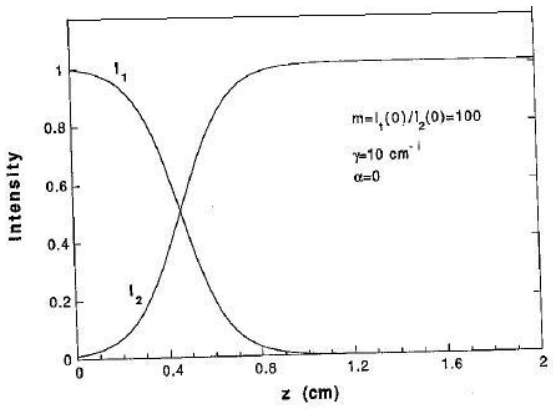

Figure 2.12: Intensities of the two beams in Co-Directional 2WM without losses, when propagation is in z-direction. Image taken from [19].

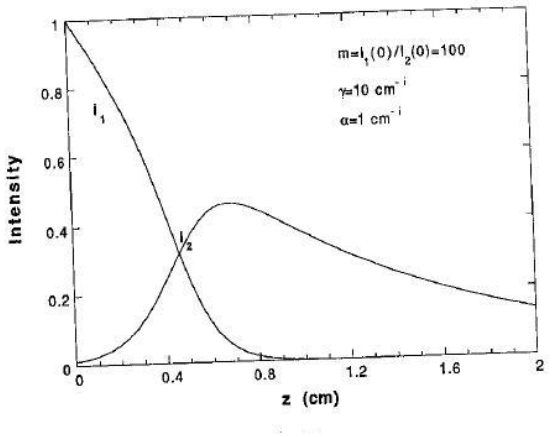

Figure 2.13: Intensities of the two beams in Co-Directional 2WM with losses, when propagation is in z-direction. Image taken from [19].

Contra-Directional TWM: $k_{1z} \cdot k_{2z} < 0$

$$\frac{d}{dz}I_1 = -\gamma \frac{I_1 I_2}{I_1 + I_2} - \alpha I_1 \tag{2.37}$$

$$\frac{d}{dz}I_2 = \gamma \frac{I_1 I_2}{I_1 + I_2} + \alpha I_2 \tag{2.38}$$

$$\frac{d}{dz}\psi_1 = \beta \frac{I_2}{I_1 + I_2} \tag{2.39}$$

$$\frac{d}{dz}\psi_2 = -\beta \frac{I_1}{I_1 + I_2} \tag{2.40}$$

β and γ as above.

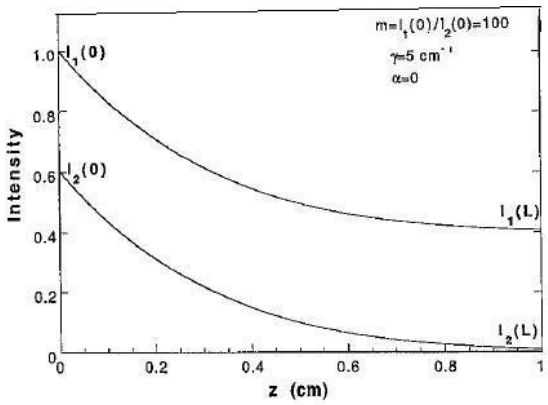

Figure 2.14: Intensities of the two beams in Co-Directional 2WM with losses, when propagation is in z-direction. Image taken from [19].

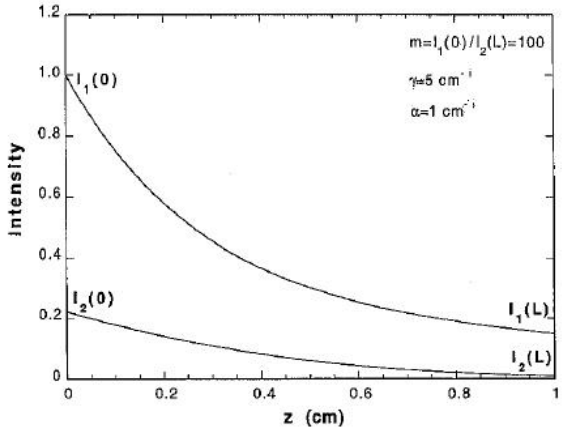

Figure 2.15: Intensities of the two beams in Co-Directional 2WM with losses, when propagation is in z-direction. Image taken from [19].

Non-Degenerate TWM - moving gratings:

The two beams have slightly different frequencies ω_a and ω_b and wavevectors $\vec{k_a}$ and $\vec{k_b}$ respectively.

$$\Delta\omega = \omega_b - \omega_a \tag{2.41}$$

$$\vec{K} = \vec{k_b} - \vec{k_a} \tag{2.42}$$

The fringe pattern produced the intersecting beams reads

$$I(\vec{r}, t) = I_0 + Re\left\{I_1 \cdot e^{i(\Delta\omega \cdot t - \vec{K}\cdot\vec{r})}\right\} \tag{2.43}$$

where I_0 and I_1 are the expressions for the static fringe pattern, equations (2.13) and (2.14).

Now the intensity pattern moves along the direction $\vec{K}$ with a velocity

$$v = \frac{\Delta\omega}{|\vec{K}|}. \tag{2.44}$$

This has consequences on the amplitude of the space charge field and on the phase shift between the intensity pattern and the space charge field.

The amplitude becomes smaller by a factor $(1 + (\Delta\omega \cdot \tau)^2)^{-1/2}$ and there is an additional time dependent phase shift introduced:

$$E_1(\Delta\omega) = \frac{|E_1(0)|}{\sqrt{1 + (\Delta\omega \cdot \tau)^2}} \cdot e^{i(\phi + tan^{-1}(\Delta\omega \cdot t))} \tag{2.45}$$

$|E_1(0)|$ and $\phi = \pi/2$... according to equation (2.17)
τ... photorefractive grating decay constant (see [19]).

These modifications are due to the finite time required to generate the index grating and trap the charge carriers.
Since the intensity fringe pattern moves, also the induced charge distribution moves. If the intensity moves fast, the material´s response might be too slow and the photorefractive effect vanishes.

The coupling constant γ of the degenerate 2WM is diminished and reads

$$\gamma = \frac{\gamma_0}{1 + (\Delta\omega \cdot \tau)^2} \tag{2.46}$$

where γ_0 is the coupling constant of degenerate 2WM.

2.4.2 Degenerate Four-Wave-Mixing (FWM) in photorefractive materials

Closed form solutions for FWM can be achieved by the grating-integral method as discussed in [19]. For reasons of illustration there are equal coupling constants assumed below.

The four intersecting beams of equal frequency are supposed to be of the form

$A_i = \sqrt{I_i} e^{-i\psi_i}$, $i = 1, 2, 3, 4$

In the case of symmetric incidence, there are four gratings G(z) produced inside the photorefractive material:

$$A1A2^* + A3A4^* \tag{2.47}$$

$$A2A4^* + A1A3^* \tag{2.48}$$

$$A1A4^* \tag{2.49}$$

$$A2A3^* \tag{2.50}$$

The first one is a transmission grating, the second one is a reflection grating and equations (2.49) and (2.50) are $2k$-gratings.

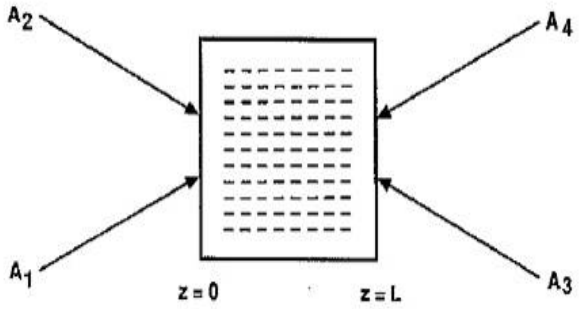

Figure 2.16: Four-Wave -Mixing via a transmission grating. The grating is formed by beam pair (A1, A2) and/or (A3, A4). Image taken from [19].

As the strength of the gratings depends on the space charge field and the polarization states of the light, usually only for one of all the gratings conditions of strong amplification are given.

Assuming that the transmission grating given by eq.(2.47) and shown in figure 2.16 predominates, the coupled equations of the FWM process read

$$\frac{d}{dz}A1 = -\frac{1}{2}\Gamma G\frac{A2}{I_0} \tag{2.51}$$

$$\frac{d}{dz}A2 = \frac{1}{2}\Gamma^* G^*\frac{A1}{I_0} \tag{2.52}$$

$$\frac{d}{dz}A3 = \frac{1}{2}\Gamma G\frac{A4}{I_0} \tag{2.53}$$

$$\frac{d}{dz}A1 = -\frac{1}{2}\Gamma^* G^*\frac{A3}{I_0} \tag{2.54}$$

$I_0 = I_1 + I_2 + I_3 + I_4$
G... transmission grating given by eq.(2.47)
Γ... FWM coupling constant

Depending on the boundary conditions there are different processes happening. The intensities of the four interacting beams of typical FWM configurations are shown in figures 2.17 and 2.18.

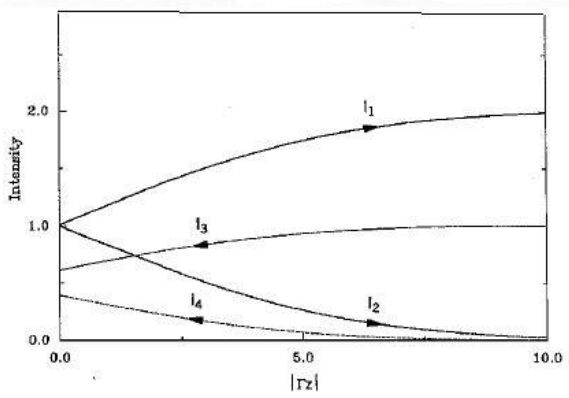

Figure 2.17: Intensities of the beams in Four-Wave-Mixing via transmission gratings. The boundary conditions are $I1(0) = I2(0) = I3(L) = 0$ and the coupling constant is $\Gamma = -1.0$. Image taken from [19].

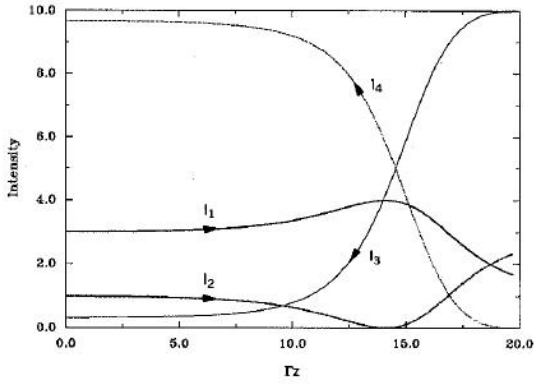

Figure 2.18: Intensities of the beams in Four-Wave-Mixing via transmission gratings. The boundary conditions are $I1(0) = 3.007, I2(0) = 1.0, I3(L) = 10.0$ and the coupling constant is $\Gamma = 1.0$. Image taken from [19].

Conditions for Oscillation in a PRO :

The basic processes in a PRO can approximately be described by Two-Wave-Mixing or Four-Wave-Mixing.

In initializing the oscillation beam fanning due to photorefractive TWM plays an crucial role.

Beam Fanning :

When the laser light of the pump beam enters in the photorefractive medium the scattered light is asymmetrical with respect to the pump beam. It grows in time until it finally reaches a steady state. This is due to energy coupling between the incident and the scattered light. Due to photorefractive TWM a large number of photo-induced gratings is formed. Conditions for strong amplification depend on the polarization state of the light and on the orientation of the crystal

causing an asymmetric scattering pattern.

When oscillation has started optical FWM happens in the resonator.
Depending on the geometry of pumping and injection beams the cavity field is described by degenerate or non-degenerate FWM in a PRO.

The order parameter equation in the case of degenerate FWM is of the form of the real Swift-Hohenberg equation (1.4).
In the case of non-degenerate FWM the oscillation is described by the complex Swift-Hohenberg equation (1.1).

Concerning detuning of the cavity, PROs show a further peculiarity with respect to lasers:
While in conventional nonlinear media the gaincurve width is several GHertz because of the Doppler broadening, the gain curve of TWM in photorefractive material is narrower than the mode spacing.

Even though the gain bandwidth of photorefractive TWM is very narrow oscillation in PROS is sustained over a large range of cavity detuning, as long as strong coupling is provided. This is explained with the *dependence of the photorefractive phase shift on the detuning of the resonator.*

Theory of a photorefractive phase shift :

The following considerations are done for a unidirectional ring resonator that is pumped with a beam of frequency ω_1, as shown in figure 2.19.

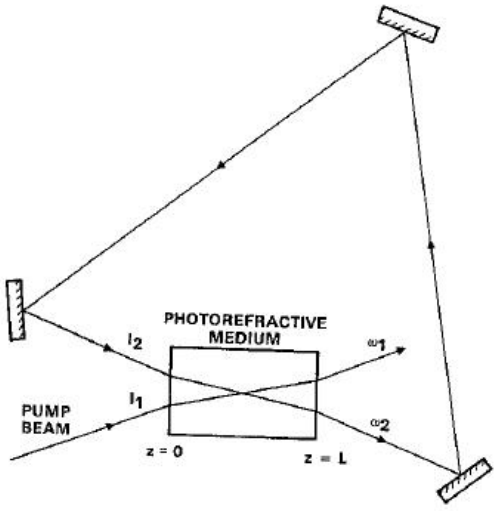

Figure 2.19: Scheme of a unidirectional ring resonator pumped by a beam with frequency ω_1. Oscillation occurs at frequency ω_2, which is determined by the resonator length. Image taken from [19].

The interaction of the pump and oscillation beams is approximately described by non-degenerate co-directional TWM (figure 2.20).

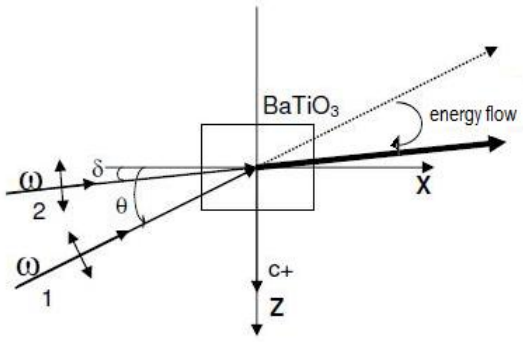

Figure 2.20: Scheme of a TWM process in $BaTiO_3$, where the direction of the energy flow for the given pumping geometry is indicated. ω_1 is the frequency of the pump beam. Oscillation occurs with ω_2 along the direction of the resonator axis. Image taken from [2].

The gain of photorefractive TWM (figure 2.21) is a function of frequency detuning between the beams. The gain is significant only for $|\Delta\omega \cdot \tau < 1|$.
For $BaTiO_3$ with an operating intensity of $1W/cm^2$ τ is between $0.1s$ and $1s$ implicating a gaincurve width of a few Hertz.

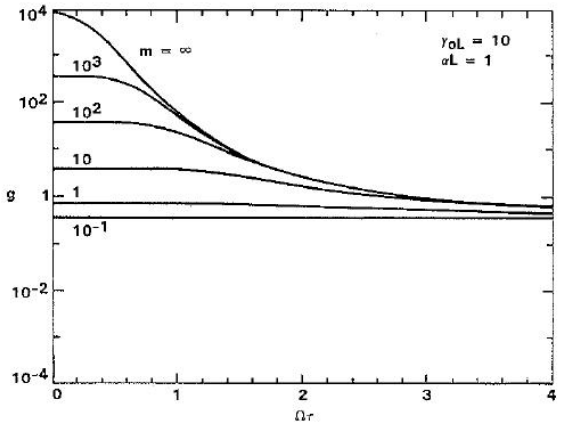

Figure 2.21: Signal gain g in co-directional degenerate TWM as a function of the frequency detuning $\Delta\omega \cdot \tau.m$ is the ratio of the beam intensities. Image taken from [19].

Experimental results in PROS in both linear and ring configuration indicate that the frequency difference between pumping an oscillating beams depends on the optical cavity length.

This supports the theory of a photorefractive phase shift which predicts that the unidirectional ring resonator can sustain conditions of resonance by introducing a phase shift and a difference in frequency between the pumping and the oscillation beam when detuned in length.

Oscillation occurs, when the gain overcomes the losses $\gamma > \alpha$ and the round-trip optical phase reproduces itself :

$$\Delta\psi + \int k \cdot ds = 2N\pi \tag{2.55}$$

$$gR = 1 \tag{2.56}$$

$\Delta\psi$...additional phase shift due to photorefractive coupling
R...total reflectivity of the cavity
g...degenerate TWM gain, given by

$$g = \frac{I_2(L)}{I_2(0)} = \frac{1+m}{1+me^{-\gamma L}}e^{-\alpha L} \tag{2.57}$$

L...interaction length
m...ratio of the beam intensities $m = \frac{I_1(0)}{I_2(0)}$
α...absorption coefficient
γ...coupling constant of non-degenerate TWM, given by

$$\gamma = \frac{\gamma_0}{1+(\Delta\omega \cdot \tau)^2} \tag{2.58}$$

$\gamma_0 = \gamma(\Delta\omega = 0)$... coupling constant of degenerate TWM, eq.(2.35).
$\Delta\omega$... frequency difference between pump and oscillating beam
τ... photorefractive time response

For a pump beam with frequency ω_1 and intensity I_1, those equations can be used to find the oscillation frequency ω_2 (or equivalently $\Delta\omega = \omega_2 + \omega_1$ and the oscillation intensity I_2:

The detuning of the resonator from the exact resonance length for ω_1 determines the necessary phase shift between the pump and oscillating beam for conditions of resonance.
Equation (2.55) can be written:

$$\Delta\Psi = \Delta\Gamma + 2M\pi \tag{2.59}$$

$\Delta\Gamma$ is the detuning of the cavity length and lies between $-\pi$ and π.

On the other hand $\Delta\Psi$ is defined by equations (2.30) - (2.36), whereas instead of eq.(2.35) the coupling constant of non-degenerate TWM eq.(2.58) has to be taken.

$$\Delta\psi = \psi_2 - \psi_1 = -\frac{\beta}{\gamma} ln\left(R \cdot e^{-\alpha L}\right) \tag{2.60}$$

Via the coupling constant γ, eq.(2.58), $\Delta\Psi$ depends on $\Delta\omega$, i.e. ω_2.

This dependence of the phaseshift due to the photorefractive coupling on the frequency difference of slightly non-degenerate TWM is shown in figure 2.22.

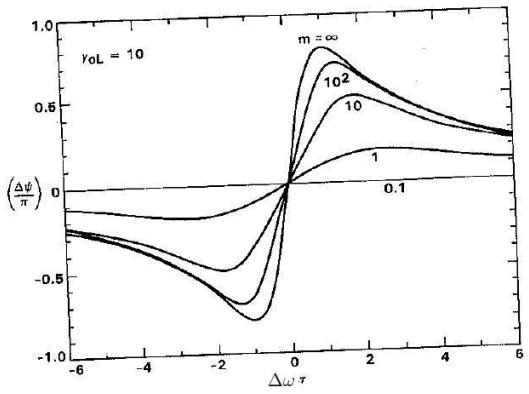

Figure 2.22: Photorefractive phase shift $\Delta\Psi$ in co-directional degenerate TWM as a function of the frequency detuning $\Delta\omega \cdot \tau.m$ is the ratio of the beam intensities $m = \frac{I_1(0)}{I_2(0)}$. Image taken from [19].

Inverting this functional dependence one finds for $\Delta\omega$:

$$\Delta\omega = [2(\Delta\Gamma + 2M\pi)/\tau A] \tag{2.61}$$

$\Delta\omega$..... frequency difference between pumping an oscillating beams
$\Delta\Gamma$...detuning of the optical resonator length
M...integer number
A...total cavity losses
τ... photorefractive time response

The detuning ranges read

$$|\Delta\omega| \leq (1/\tau)(\gamma_0 L/A - 1)^{1/2} \tag{2.62}$$

$$|\Delta\Gamma| \leq (A/2)(\gamma_0 L/A - 1)^{1/2} \tag{2.63}$$

L...interaction length
$\gamma_0 = \gamma(\Delta\omega = 0)$... coupling constant of degenerate TWM, eq.(2.35).

Form eq.(2.62) one sees, that strong coupling γ_0 leads to a wide range of possible frequency detuning. If the detuning becomes too large oscillation ceases.

2.5 The Experimental Setup

I: In a first part of the planned experiment the Spatial Rocking technique (section 1.9.3) should have been applied to a PRO in non-degenerate FWM configuration (figure 2.23). In this configuration the PRO represents a phase invariant system (see section 1.8) and characteristic structures are vortices (figures 1.8, 1.9 and 1.27 a) and tilted waves (figure 1.16).
In such a system Spatial Rocking is supposed to break the phase invariance and convert the free system into a bistable one described by equation (1.17). The bistable optical field can take only two phase values (separated by π radians), while the amplitude is the same for both states (figures 1.12 left column and 1.26 b).
If spatially extended one region can take one phase and the rest the opposite phase. Stripes are the characteristic extended pattern of regions of constant phase. Two regions of opposite phase are separated by a local structure called domain wall, which can be of the Ising or Bloch type (figures 1.27 b and c). Those walls usually move but stationary solutions of these domain walls exist and are called dark solitons (figures 1.31 and 1.21 e.g.). Solitons are found for certain cavity parameter values (see section 1.8).

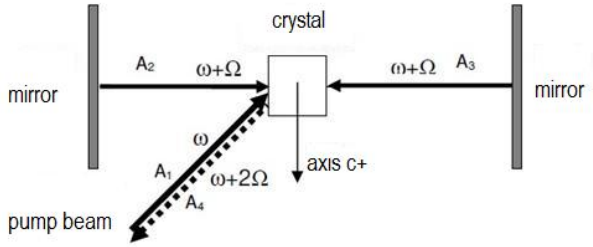

Figure 2.23: Schematic representation of non-degenerate FWM in a PRO.

II: In a next step Spatial Rocking would have been applied to a PRO in degenerate FWM configuration (figure 2.24). This is achieved with a pair of equivalent counter-propagating pump beams. A PRO in degenerate FWM configuration is bistable in phase even without Rocking being applied and the cavity field is described by equation (1.4). When Rocking is applied there are four equivalent states with phase values separated by $\pi/2$ expected, making the system four-phase multistabe.

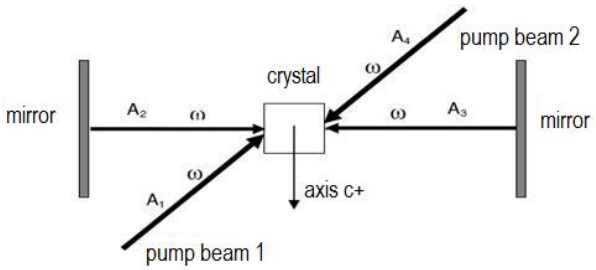

Figure 2.24: Schematic representation of degenerate FWM in a PRO.

Part I: Rocking of a PRO in degenerate FWM configuration

To study the nonlinear patterns described by the CSHE and RSHE we need to realize a single-longitudinal multi-transversal mode inside the PRO where diffraction due to the devices can be neglected (see also 2.2).

For this sake we seek

- a large Fresnel-number
- and a perturbation free signal.

The first requirement can be satisfied using a *quasi-self-imaging* configuration (see end of the section) and the second one by a *pneumatic table* and an *electric stability control*.

We expected to observe the same structures as in the Temporal Rocking experiments. That are vortices and solitons in the free and the rocked system, respectively. Figure 2.25 shows experimental data of a Temporal Rocking experiment as it was performed in [6]. Figure **??**) shows vortices that we could obeserve in our experiment without Rocking beeing applied.

The dynamics and kind of patterns should have been studied under the influence of the detuning between the pump beam and oscillating beam $\Delta\omega = \omega_{pump} - \omega_{cavity}$ and the modulation frequency of the Rocking signal.

The experimental setup is shown in figures 2.26 to 2.29.

The resonator is divided in an active and passive branch. Both branches are linear Fabry-Perot resonators in quasi-auto-imaging configuration. Auto-imaging is described in detail at the end of the section.
The active branch carries the nonlinear crystal (figure 2.29), while the passive branch is empty (figure 2.29 whithout the $BaTiO_3$ crystal). Experimentally this is realized by introducing a quadratic geometry into the cavity field as presented in figure 2.27.

Even though in linear configuration there is gain in one direction but losses in the opposite direction. Nonetheless the linear resonator is chosen instead of a ring configuration out of practical reasons.

Figures 2.27 and 2.26 show the basic components of the Rocking experiment. Of course additional devices can be used to achieve better results in the produced images.

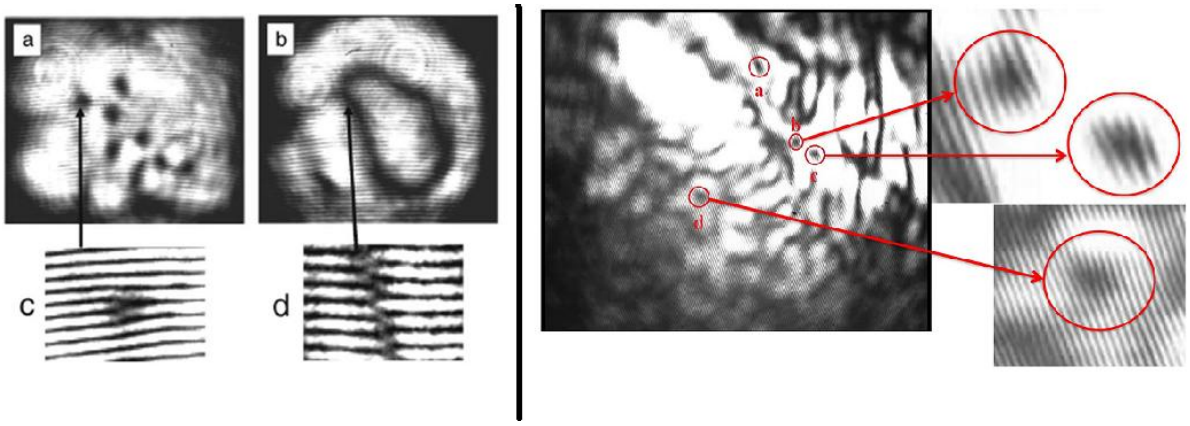

Figure 2.25: Left: Holographic image of the transverse plane of the near field of the crystal in a Temporal Rocking experiment. Vortices (left) appear, when Rocking is not applied while domain walls (right) appear when Rocking is applied. The detailed view of the phase patterns show that c) at the site of a vortex two fringes of the interferogram are converted into one, which is characteristic for the singularity in phase at the site of the defect and d) that two periodic fringe patterns, each representing a particular phase value, are shifted by π radians at the site of the domain wall. Image taken from [6]. Right: Holographic image of our experiment without Rocking beeing applied. Left: Vortices appear in the transverse plane of near field of the crystal. Right: Detailed view. On the site of a vortex two fringes of the interferogram are converted into one, which is characteristic for the singularity in phase at the site of the defect. Image taken from [28].

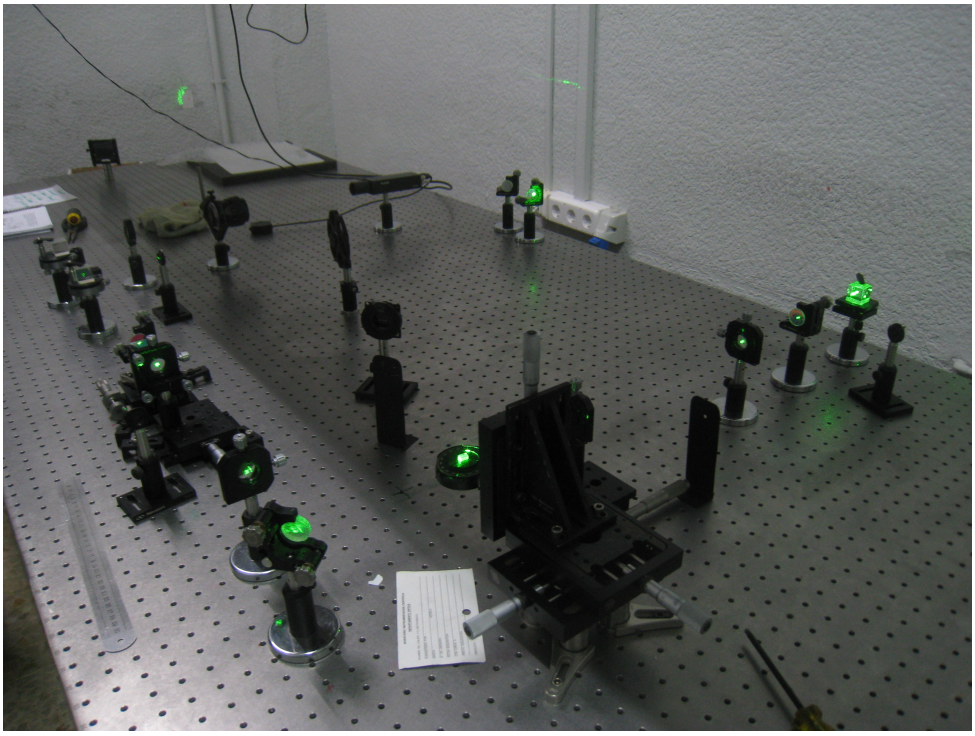

Figure 2.26: Experimental setup for the Spatial Rocking Experiment. Photorefractive Resonator in degenerate FWM configuration with BaTi03 as active medium. Image taken in the Optical Department of the University of Valencia.

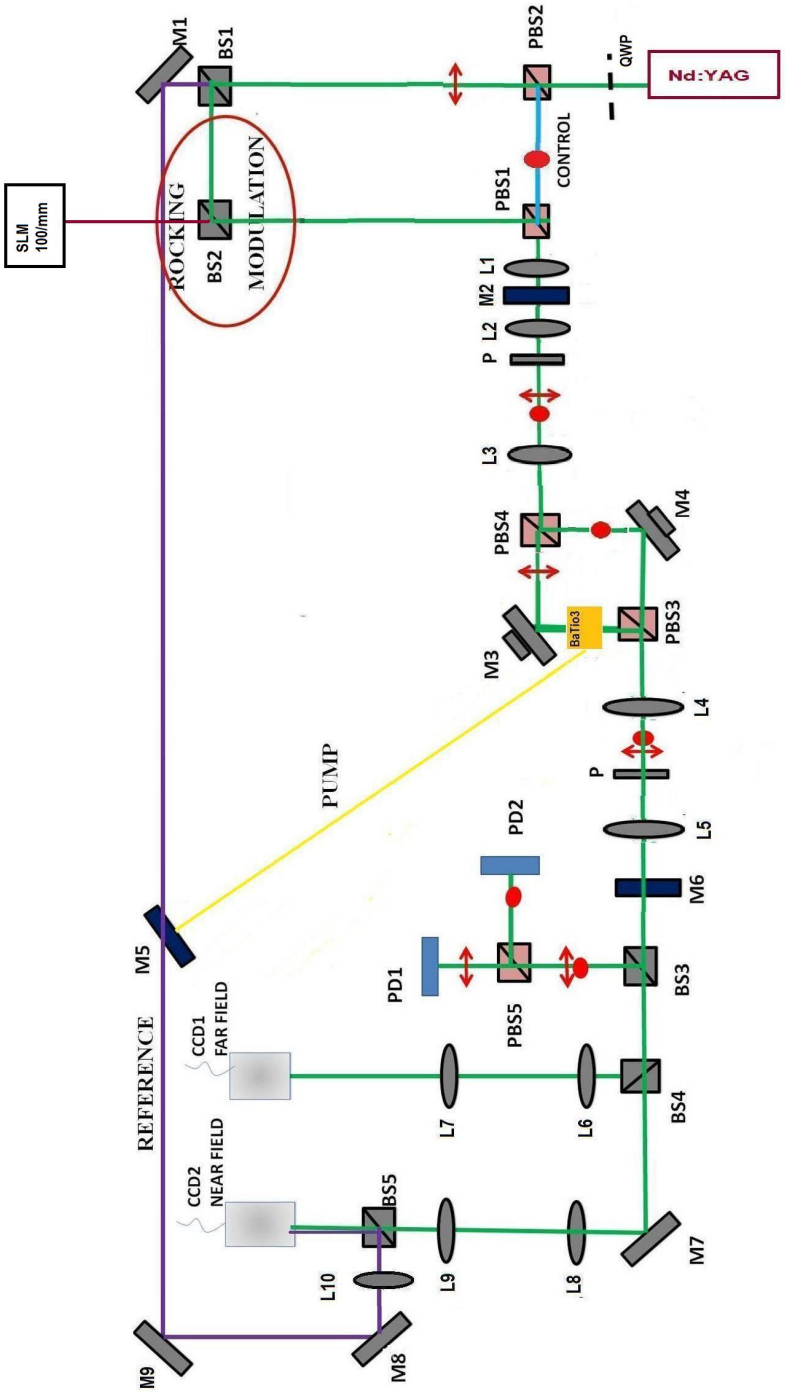

Figure 2.27: Schematic setup for the Spatial Rocking Experiment. Photorefractive Resonator in degenerate FWM configuration.

Devices:

The light source is a Nd:YAG laser. For the experiment we use a power of $P = 10mW$. Frequency doubling is done to achieve emission at $\lambda = 523nm$. The light is linearly polarized in horizontal direction.
In the chosen position of the $BaTiO_3$ the horizontal light corresponds to the extraordinary polarization ($n_e \approx 2.4$).

QWP.... quarter-wave plate to produce a polarization at 45°

PBS1,PBS2,PBS3,PBS4, PBS5 .... polarization beam splitters (high reflectivity)

PBS1 ..... divides the light polarized at 45° into its horizontal and vertical parts, marked as red fletcher and red dot, respectively. The vertically polarized light is sent to the control cavity. The horizontally polarized light is separated by beam splitter BS1. One part is used as reference beam the other part is supposed to be modulated with the Rocking signal and sent to the active cavity

PBS3, PBS4, M3, M4.... the two beam splitters and the two mirrors provide the separation of the cavity field into an active and a passive branch. The polarization beam splitter PBS3 divides the beam into its horizontal and vertical parts. The horizontally polarized light gets bent by mirror M3 and is sent through the $BaTiO_3$ crystal (active branch), the vertically polarized light gets bent by mirror M4 and passes through the empty branch. Beam splitter PBS4 unites the two parts again.

PBS5.... separates the signal of the active cavity from the one of the control cavity and sends the two parts to the corresponding entrance of the lock in amplifier

BS1.... beam splitter to divide the vertically polarized light into a reference and an experimental beam
BS2.... on the site of this beam splitter the Spatial Rocking signal, coming from the SLM device, will be introduced

BS3.... beam splitter to sent part of the signal beam to the entrance of the lock in amplifier PD1

BS4.... beam splitter to sent part of the signal beam to the far field detection

BS5.... unites the reference beam with the signal beam to produce interferometric information at the site of the near field detector CCD2

M1,M2,M3,M6,M7,M8,M9 ..... plane mirrors of circular shape and a reflectivity of 95%

M2,M6....plane mirrors of circular shape and a reflectivity of 95% constituting the resonator M6 can be moved, which determines the effective length of the quasi-auto-imaging configuration (see end of the section)

M3.... piezoelectric mirror to change the length of the active cavity branch.
By application of DC voltage detuning of the active cavity is achieved

M4.... as M3, but for the control cavity

M5.... semitransparent mirror to separate a part of the reference beam and send it as pump beam to the crystal

L1..... convex lens to introduce a slight divergence into the collimated monofrequent source beam before injecting it into the resonator
This implicates FWM in several directions within the resonator to achieve an extended system as described in section 2.2.

L2,L3,L4,L5.... pairs (L2,L3) and (L4,L5) of convex lenses, constituting the telescope systems of the self-imaging-configuration (see 2.5)
L6,L7,L8,L9.... lens system (L6,L7) and (L8,L9) to focus the near and far field information contained in the planes through the crystal center and the focal planes of the telescope systems on the plane of the charge coupled devices CCD2 and CCD1 respectively

L10.... convex lens to align the signal and the reference beam in order to achieve coherence
SLM.... Spatial light modulator. This is a spatial light grating of high frequency ($\approx 100/mm$), which is designed by Matlab.

PD1.... entrance of the lock in amplifier that records the signal of the active cavity

PD2.... exit of the lock in amplifier that provides a sinusoidal signal to the passive cavity

CCD1... charge coupled device to record the far field (Fourier space)

CCD2... charge coupled device to record the near field (crystal plane)

P.... circular diafragms in the focal planes of the telescope systems which allow filtering of high spatial frequencies in the Fourier-space

Beams:

All the beams have intensities in the order of 10 mW. The source is set to emit at 10 mW and the source beam is separated by beam splitters into the following beams:

The **rocking beam (dark green)** is injected parallel to the optical axis of the resonator. It is horizontally polarized and spatially modulated via a spatial light modulator (SLM).

The **reference beam (dark blue)** is horizontally polarized as the rocking and signal beams. It is directly sent to the near field detector CCD2.

The **control beam (light blue)** is vertically polarized. It is sent to the empty branch of the cavity and the control signal is sent to the lock-in amplifier.

The **pump beam (yellow)** is horizontally polarized.
The optimal angle of incidence is about $\theta = 50°$ for the position of the crystal inside the resonator as presented in figure 2.28. The axis of the crystal should form an angle $\delta = 5°$ with respect to the resonator axis.

For the sake of optimal adjustment the empty resonator has to be aligned first. Then the crystal is put into one of the two branches of the cavity and slightly gyrated clockwise (about 5°). As a next step the pump beam is turned on and the angle of incidence is varied such that the via beam fanning (see sec.2.4.2) dispersed light is most intensive in the direction of the resonator axis.

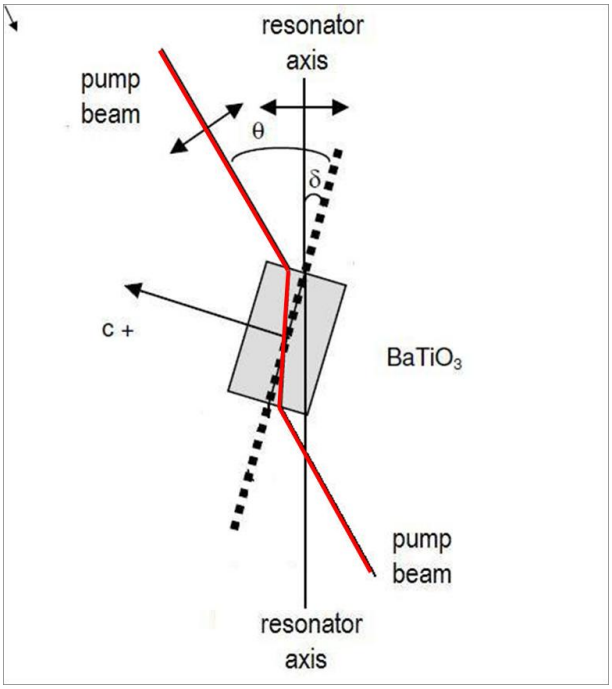

Figure 2.28: Scheme of the position of the $BaTiO_3$ crystal inside the resonator and geometry of the pumping for optimal beam coupling.

The **signal beam** appears to be horizontally polarized as well.

The lock-in amplifier:
To stabilize the active cavity against fluctuations and vibrations, the resonator is constructed as double cavity. While the active branch contains the $BaTiO_3$ crystal the control cavity is empty. Both approximately have the same effective length.

The piezoelectric mirror M4 of the control cavity is connected to a sinusoidal signal provided by the lock-in amplifier (exit PD2).
The signal of the control cavity is then compared to the signal of the active cavity and the feedback is put on the piezoelectric mirror M3F which is located in the active cavity.

The **near field recording system** consist in a lens-system represented by lenses L8 and L9 and the photosensitive charge coupled device CCD2. It is focused on the plane through the center of the $BaTiO_3$ crystal. The signal beam is super-posed with the reference beam such that the interference pattern recorded by this holographic techniques contains information about the phase and amplitude of the vacity field. The phase is reconstructed from the interference pattern with an appropiate analyzing programme. Phase structures as vortices and domain walls are seen on these records.

The **far field recording system** consist in a lens-system represented by lenses L6 and L7 and the photosensitive charge coupled device CCD1. It is focused on the focal plane of the telescope system (FP2 in figure 2.5) and records the spatial frequency spectrum of the signal beam.

Self-Imaging

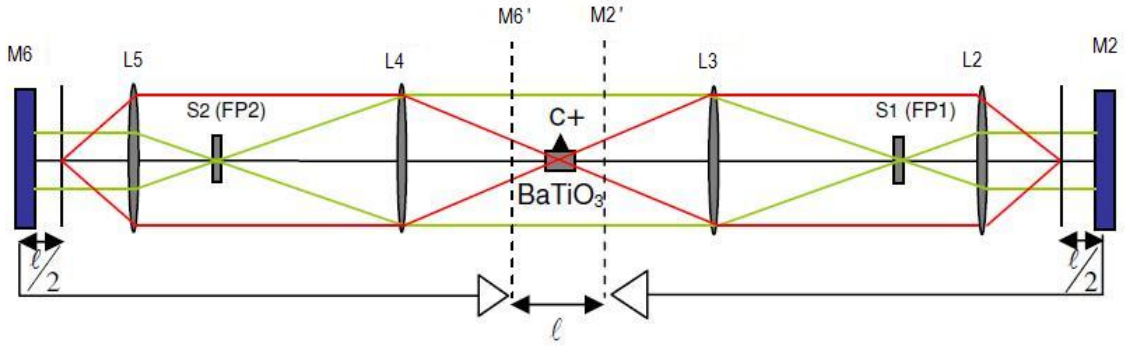

Figure 2.29: Scheme of a Fabry-Perot resonator in quasi-auto-imaging configuration. The denomination of the devices refers to figure 2.27. l is the effective cavity length given by the distance between the images $M2'$ and $M6'$ of the mirrors M2 and M6.

In this kind of resonator images of the resonator mirrors are formed via a lens system (telescope system) in such a manner, that the real resonator becomes an effective one with an effective length much smaller than the real length. Inclusive zero and negative effective lengths are possible.

In the case of zero effective resonator length the configuration is called auto-imaging or self-imaging and in the case of small effective lengths one talks of quasi self-imaging.

In this setup the far field is accessible on the experimental desk as it corresponds to the focal planes (FP1 and FP2 in figure 2.29).

In our case the total length of the resonator as defined by the distance between the mirrors M2 and M6 is

$L = 124.5 + 0.1$ cm.

With the two telescope systems formed by lenses (L2,L3) and (L4,L5) in the position as presented in figure 2.29 an effective length of
$l = 4.5 + 0.1$ cm

is obtained.

CHAPTER 3

Acknowledgements

I really want to thank the Optical group in Valencia.
First of all Fernando for the help in all aspects and the possibility to follow the many questions that seemed so important to be answered before the experimental work could start.
Germán for the great seminar and lecture which allowed such a pictorial access to quantum optics.
Eugenio for the good explanations and the confidence, when theory seemed to become too confusing.
Rubén for the great company and the advices concerning writing a thesis and for the patience, when theoretical preoccupations impeded trial and fail.
Javier for letting us take a sip of his incredibly large pool of experience and knowledge in the laboratory.
Marta for the motivation and practical tips and the shared breaks.
All the others for the good impulses, the help, the interesting discussions and for being such a nice group!
Laurentius Windholz for allowing so much room for the realization of this Master´s thesis.
Thanks to Günter for helping me so much with the formalisms and for the prospering exchange of experiences!
Finally I really want to thank my family and my friends in Austria for all their support!

Bibliography

[1] Germán J. de Valcárcel and Kestutis Staliunas, Patter Formation through Phase Bistability in OScillatory Systems with Space-Modulated Forcing,Phys. Rev. Lett., PRL 105, 054101 (2010)

[2] Esteban Martín, Adolfo: Docotoral Thesis, Generación y Caracterización Experimentales de Estructuras Disipativas en Osciladores Fotorrefractivos (Experimental Generation and Characterization of Dissipative Structures in Fotorefractive Oscillators), Valencia, Spain, March 2006.

[3] K. Staliunas, G. Slekys, and C. O. Weiss, Phys. Rev. Lett. 79, 2658 (1997).

[4] G.J. de Valcárcel and K. Staliunas, Excitation of phase patterns and phase solitons via two frequency forcing of a 1:1 resonance, Phys. Rev. E 67, 026604 (2004).

[5] V.B. Taranenko, K. Staliunas, and C.O. Weiss, Pattern formation and localized structures in degenerate optical parametric mixing, Phys. Rev. Lett. 81, 2236 (1998).

[6] Adolfo Esteban-Martín, Manuel Martínez-Quesada, Victor B. Taranenko, Eugenio Roldán, Germán J. de Valcárcel, Bistable Phase Locking of a nonlinear Optical Cavity via Rocking: Transmuting Vortices into Phase Patterns, Phys. Rev. Lett. PRL 97, 093903 (2006).

[7] K. Staliunas, G.J. de Valcárcel, M. Martínez-Quesada, S.Gilliand, A. González-Segura, G. Munoz-Matutano, J. Cascante-Vindas, J. Marqués-Hueso, S. Torres-Peiro, Bistable phase locking in rocked lasers, Science Direct, Optics Communications 268 (2006) 160-168

[8] K. Staliunas, M. F. H. Tarroja, G. Slekys and C.O. Weiss, Analogy between photorefractive oscillators and class-A lasers, Phys. Rev. A 51, n°5 (1995)

[9] H. Joachim Schlichting. WWU Mün Praxis der Naturwissenschaften/ Physik 49/2 (2000); 12- 16

[10] D. Neshev, A. Dreischuh, V. Kamenov, I. Stefanov, S. Dinev, W. Fließer, L. Windholz, Generation and intrinsic dynamics of ring dark solitary waves, Appl. Phys. B 64, 429-433 (1997)

[11] M.C. Cross and P.C. Hohenberg, Pattern formation outside of equilibrium, Rev. Mod. Phys. 65, 851(1993).

[12] R. Graham and H. Haken, Laserlight first example of a second order phase transition far from thermal equilibrium, Z. Phys. 237, 31 (1970).

[13] S.A. Akhmanov, R.V. Khoklov, and A.P. Sukhorukov, in Laser Handbook, ed. by F.T. Arechi and E.O. Schultz-DuBois (North-Holland, Amsterdam, 1972).

[14] L.A. Lugiato, C. Oldano, and L.M. Narducci, Cooperative frequency locking and stationary spatial structures in a laser, J. Opt. Soc. Am. B 5, 879 (1988).

[15] L.A. Lugiato, G.L. Oppo, J.R. Tredicce, L.M. Narducci, and M.A. Pernigo, Instabilities and spatial complexity in a laser, J. Opt. Soc. Am B 7, 1019 (1990).

[16] P. Coullet, L. Gil, and F. Rocca, Optical vortices, Opt. Commun. 73, 403 (1989).

[17] Lecture Notes from the Optics Seminar of Germán J. de Valcárcel, Department of Optics, Valencia, October 2012

[18] Boyd, Robert W.: Nonlinear Optics, Academic Press, Rochester, New York, October, 2007.

[19] Yeh, Pochi: Introduction to Photorefractive Nonlinear Optics, John Wiley & Sons, Inc., Thousand Oaks, California, January, 1993.

[20] Lexikon der Physik; Walter Greulich [Hrsg.]; ISBN 3-86025-291-7

[21] Laser; Bauformen, Strahlführung, Anwendungen; Jürgen & Hans Joachim Eichler; ISBN 978-3-642-10461-9

[22] Optik; Eugene Hecht; ISBN 978-3-486-58861-3

[23] Thermodynamics; Honig, Jürgen M.; ISBN 978-0-12-416705-6

[24] Ice crystals, Elisabeth Rogl, 2010

[25] Coral snake and giraffe; bing.com/images , Microscipic fotography; Helga Rogl

[26] From above to bottom, from left to right: Earth; NASA, Salt lake of Uyuni; Elisabeth Rogl, Bolivia, 2007, Experimental Setup; Eliabeth Rogl, Laboratory of the Optics Department, Valencia, 2013, V.B. Taranenko, K. Staliunas, and C.O. Weiss; Pattern formation and localized structures in degenerate optical parametric mixing, Phys. Rev. Lett. 81, 2236 (1998).

[27] Soliton wave in water, observed by Univ.-Prof. Dipl.-Ing. Dr.techn. Laurentius Windholz

[28] Rubén Martínez Lorente, Laboratory of the Optics Department, Valencia, 2013